

# ornl

OAK RIDGE  
NATIONAL  
LABORATORY

MARTIN MARIETTA

MARTIN MARIETTA ENERGY SYSTEMS LIBRARIES



3 4456 0278072 9

ORNL/TM-10327

## A Modeling Study of Vacuum Sorption Characteristics of Carbon Dioxide on 4A Zeolite Molecular Sieves

J. K. Prazniak  
C. H. Byers

OAK RIDGE NATIONAL LABORATORY

CENTRAL RESEARCH LIBRARY

CIRCULATION SECTION

ISSUE ROOM 175

**LIBRARY LOAN COPY**

DO NOT TRANSFER TO ANOTHER PERSON

If you wish someone else to see this  
report, send in name with report and  
the library will arrange a loan.

FORM 7203 12-67

OPERATED BY  
MARTIN MARIETTA ENERGY SYSTEMS, INC.  
FOR THE UNITED STATES  
DEPARTMENT OF ENERGY

Printed in the United States of America. Available from  
National Technical Information Service  
U.S. Department of Commerce  
5285 Port Royal Road, Springfield, Virginia 22161  
NTIS price codes—Printed Copy: A05 Microfiche A01

This report was prepared as an account of work sponsored by an agency of the United States Government. Neither the United States Government nor any agency thereof, nor any of their employees, makes any warranty, express or implied, or assumes any legal liability or responsibility for the accuracy, completeness, or usefulness of any information, apparatus, product, or process disclosed, or represents that its use would not infringe privately owned rights. Reference herein to any specific commercial product, process, or service by trade name, trademark, manufacturer, or otherwise, does not necessarily constitute or imply its endorsement, recommendation, or favoring by the United States Government or any agency thereof. The views and opinions of authors expressed herein do not necessarily state or reflect those of the United States Government or any agency thereof.

Chemical Technology Division

**A MODELING STUDY OF VACUUM SORPTION CHARACTERISTICS  
OF CARBON DIOXIDE ON 4A ZEOLITE MOLECULAR SIEVES**

J. K. Prazniak\*  
C. H. Byers

---

\* Health, Safety, Environment, and Accountability Division,  
Y-12 Plant Site, Oak Ridge Complex.

This report was prepared as a thesis and  
submitted to the faculty of the Graduate School  
of the University of Tennessee in partial fulfillment  
of the Master of Science in the  
Department of Chemical Engineering.

**Date of Issue - August 1987**

Prepared by the  
OAK RIDGE NATIONAL LABORATORY  
Oak Ridge, Tennessee 37831  
operated by  
MARTIN MARIETTA ENERGY SYSTEMS, INC.  
for the  
U.S. DEPARTMENT OF ENERGY  
under contract DE-AC05-84OR21400



3 4456 0278072 9



## TABLE OF CONTENTS

LIST OF TABLES.....	iv
LIST OF FIGURES.....	v
LIST OF SYMBOLS.....	vii
ABSTRACT.....	1
1. INTRODUCTION.....	2
2. LITERATURE SURVEY.....	10
2.1 Zeolite Molecular Sieves and Cryosorption Pumping.....	10
2.2 Modelling of Adsorption and Cryosorption Pumping.....	11
2.3 Numerical Methods.....	12
3. THEORY.....	14
3.1 Cryosorption Pump Model Equations.....	14
3.2 Numerical Solution.....	22
3.3 Application of Orthogonal Collocation.....	23
3.4 Solution of the Model Equations.....	26
4. RESULTS.....	30
4.1 Orthogonal Collocation with the Model of Crabb and Perona.....	30
4.2 Comparison of Proposed Model and Experimental Results.....	35
4.3 Sensitivity of CO <sub>2</sub> Results to Model Parameters.....	51
5 CONCLUSIONS AND RECOMMENDATIONS.....	57
REFERENCES.....	59
APPENDIX A. Equation-Development by Orthogonal Collocation.....	63
APPENDIX B. FORTRAN Computer Code.....	69

## LIST OF TABLES

TABLE	PAGE
1. Experimental runs of Crabb and Perona analyzed in this study .....	36
2. Constants and parameters used in the cryosorption pump model .....	37
3. Comparison of model parameters used to obtain initial and adjusted results .....	42
4. Observed and predicted run time and $\Delta P_{\max}$ as a function of feed rate and bed height or particle diameter .....	54
5. Computed effects of $k$ , $q_m$ , and $r_p$ on run time and maximum pressure drop .....	55

## LIST OF FIGURES

FIGURE	PAGE
1. Views of construction and spacing for the zeolite 4A crystalline structure .....	4
2. Apparatus used by Crabb and Perona (1985) in N <sub>2</sub> and CO <sub>2</sub> cryosorption experiments .....	6
3. Adsorption data that are typical of results obtained by Crabb and Perona in their experiments with CO <sub>2</sub> .....	7
4. Primary components of the experimental adsorption apparatus used by Crabb and Perona (1985) .....	15
5. The effect of the number of bed collocation points on the computed solution for a typical CO <sub>2</sub> run of Crabb and Perona (1985) .....	28
6. Predicted vs. Observed results for N <sub>2</sub> reported by Crabb and Perona (1985) for Run 208. ....	31
7. Predicted vs. Observed results for CO <sub>2</sub> reported by Crabb and Perona (1985) for Run 218. ....	32
8. Comparison of finite-difference and orthogonal collocation solutions to the model of Crabb and Perona (1985) for Run 208 with N <sub>2</sub> . ....	34
9. Comparison of computed and observed results for CO <sub>2</sub> [experimental data from Crabb and Perona run 218; computed results from proposed model using parameters from Table 2] .....	39
10. Comparison of computed and observed results for N <sub>2</sub> [experimental data from Crabb and Perona run 208; computed results from proposed model using parameters from Table 2] .....	40
11. Comparison of computed and observed results for CO <sub>2</sub> [experimental data from Crabb and Perona (1985) Run 217; computed results from proposed model using adjusted parameters shown in Table 3] .....	43
12. Comparison of computed and observed results for CO <sub>2</sub> [experimental data from Crabb and Perona (1985) Run 218; computed results from proposed model using adjusted parameters shown in Table 3] .....	44

13. Comparison of computed and observed results for CO <sub>2</sub> [experimental data from Crabb and Perona (1985) Run 225; computed results from proposed model using adjusted parameters shown in Table 3] .....	45
14. Comparison of computed and observed results for CO <sub>2</sub> [experimental data from Crabb and Perona (1985) Run 227; computed results from proposed model using adjusted parameters shown in Table 3] .....	46
15. Comparison of computed and observed results for N <sub>2</sub> [experimental data from Crabb and Perona (1985) Run 208; computed results from proposed model using adjusted parameters shown in Table 3] .....	48
16. Comparison of computed and observed results for N <sub>2</sub> [experimental data from Crabb and Perona (1985) Run 237; computed results from proposed model using adjusted parameters shown in Table 3] .....	49
17. Comparison of computed and observed results for N <sub>2</sub> [experimental data from Crabb and Perona (1985) Run 238; computed results from proposed model using adjusted parameters shown in Table 3] .....	50
18. Computed sorbate concentration profile in the solid for dimensionless times up to 0.5. Based on Runs 208 and 218 using parameters from Table 3 .....	52

## LIST OF SYMBOLS

$a$	Polynomial coefficient in trial solution, torr
$A$	Cross-sectional area of bed, $\text{cm}^2$
$\overline{AG}$	Discretization matrix for gas, $\text{cm}^{-1}$
$\overline{AS}$	Discretization matrix for solid, $\text{cm}^{-1}$
$b_i$	Polynomial coefficient in trial solution, mol/g molecular sieve
$c$	Concentration of gas, $\text{mol}/\text{cm}^3$
$c_i$	Orthogonal polynomial coefficient in trial solution, torr
$d$	Molecular diameter [in Eq. (10)], cm
$d$	Orthogonal polynomial coefficient in trial solution, mol/g molecular sieve
$D$	General diffusivity of sorbate in sorbent particle [Eq. (46)], $\text{cm}^2/\text{s}$
$D_0$	Corrected diffusivity, $\text{cm}^2/\text{s}$
$D_K$	Knudsen diffusivity, $\text{cm}^2/\text{s}$
$D_M$	Molecular diffusivity, $\text{cm}^2/\text{s}$
$D_p$	Pore diffusivity for bed, $\text{cm}^2/\text{s}$
$D_{\text{Pois}}$	Poiseuille diffusivity, $\text{cm}^2/\text{s}$
$D_z$	Zeolitic diffusivity, $\text{cm}^2/\text{s}$
$k$	Langmuir equilibrium constant, $\text{torr}^{-1}$
$k_B$	Boltzmann constant, J/K
$l_i$	LaGrangian polynomial coefficients (App. A)
$L$	Length of bed, cm
$M$	Number of interior collocation points in solid phase, or molecular weight of sorbate, mol/g
$n$	Number of moles in ideal gas equation
$N$	Number of interior collocation points in gas phase
$p$	Column pressure, torr
$\hat{p}$	Column pressure ratio, $p/p_r$
$p_r$	Reference pressure, torr
$\Delta p_{\text{max}}$	Maximum pressure drop, torr
$q$	Point solid loading in sorbent particle, mol sorbed gas /g molecular sieve
$\bar{q}$	Average solid loading in sorbent particle, mol sorbed gas /g molecular sieve
$\hat{q}$	Solid loading, $q/q_m$
$q_m$	Langmuir saturation constant, mol/g molecular sieve
$Q$	Flow into headspace, $\text{torr}\cdot\text{L}/\text{s}$
$r$	Radial position in sorbent particle, cm
$\hat{r}$	Radial distance ratio, $r/R$
$r_p$	Mean pore radius, cm

$R$	Sorbent particle radius, cm, or
$R$	Gas constant, torr·L/mol·K
$t$	Time, s
$T_a$	Ambient temperature, K
$T$	Bed and sorbate temperature, K
$v$	Gas velocity through bed, cm/s
$V$	Volume, cm <sup>3</sup>
$x, x_i$	General independent variable in orthogonal polynomial
$z$	Axial distance along bed, cm
$\hat{z}$	Axial distance, $z/L$

### Greek Letters

$\alpha$	Exponent in Jacobi polynomial relationship
$\beta$	Exponent in Jacobi polynomial relationship
$\lambda$	Mean free path, cm
$\epsilon$	Fraction of bed available to gas, cm <sup>3</sup> void/cm <sup>3</sup> bed
$\sigma$	Lennard-Jones collision diameter, m <sup>-10</sup>
$\theta_z$	Zeolite crystal surface area to volume ratio, cm <sup>2</sup> /cm <sup>3</sup>
$\theta_G$	Fraction of bed available to gas, cm <sup>3</sup> void/cm <sup>3</sup> bed
$\rho_b$	Bulk density of molecular sieve, g/cm <sup>3</sup> bed
$\gamma$	Polynomial expansion coefficients
$\phi_z$	Sorbent fraction of bed volume, cm <sup>3</sup> sorbent /cm <sup>3</sup> bed
$\mu$	Gas viscosity, g·cm/s
$\Omega$	Lennard-Jones collision potential function

**A MODELING STUDY OF VACUUM SORPTION  
CHARACTERISTICS OF CARBON DIOXIDE  
ON 4A ZEOLITE MOLECULAR SIEVES**

JOHN K. PRAZNAK  
CHARLES H. BYERS

**ABSTRACT**

A model is presented to describe the isothermal adsorption of carbon dioxide ( $\text{CO}_2$ ) and of nitrogen ( $\text{N}_2$ ) on 4A zeolite molecular sieves under cryogenic conditions. The model is comprised of a fluid-phase mass balance representing the dynamics of gas in the bed and a one-dimensional diffusion equation representing adsorption in the solid. Cubic crystals of 4A zeolite are assumed to be spherical, and the concentration dependence of the diffusivity of the sorbate in both the gas and solid phases is considered. Numerical solution of the parabolic partial differential model equations is accomplished using orthogonal collocation in conjunction with an ordinary differential equation integrator suitable for stiff equations.

Langmuir's adsorption isotherm is used to represent equilibrium concentrations at the gas-sorbent interface. The primary diffusional resistance is assumed to occur in the microporous zeolite crystals, rather than in the bed interstices or macropores formed by the clay binder used to pelletize the crystals. This is in contrast to the assumption of macropore resistance used in the precursory experimental and theoretical work of Crabb et al. (1986) at the Oak Ridge National Laboratory.

Experimental results obtained by Crabb et al. are compared with the theoretical results obtained by the proposed model. Good agreement with experimental results for  $\text{CO}_2$  cryosorption was obtained by increasing the Langmuir saturation constant to 20% greater than the value estimated by Crabb and Perona (1985) and by specifying an effective value for the mean pore radius of gas flow channels in the bed. The lack of agreement between theoretical and experimental results for  $\text{N}_2$  cryosorption supports a conclusion reached earlier by Crabb et al. that the controlling diffusional resistance for  $\text{N}_2$  cryosorption is in the bed interstices and micropores.

## 1. INTRODUCTION

Cryosorption pumping is a method of evacuating an enclosure by adsorbing the contained gases on a refrigerated solid sorbent. Investigators have typically studied the sorption behavior of air at temperatures from 77 K to 100 K, but new applications have emphasized the sorption of individual gases as well. Helium and hydrogen are of current interest in the study of fusion reactors, where large volumes of those gases must be removed from magnetic and radioactive environments. Experiments to study the cryopumping of hydrogen and helium have been carried out at temperatures as low as 4.2 K (Fisher and Watson 1976). Cryosorption pumps have also been employed to remove argon used in the sputter coating of semiconductor devices (Dennison and Gray, 1979). Such pumps can also be used to adsorb and hold hazardous gases from hazardous or gases from remote areas temporarily until a disposition can be determined (Wheeler 1974).

Various sorbents may be used in cryopumping applications, but zeolite molecular sieves are preferred because of their high pumping speed, physical stability, and chemical inertness. Zeolites are crystalline aluminosilicate compounds composed of a highly structured three-dimensional framework of silicon tetrahedra and aluminum tetrahedra or octahedra. Different arrangements of the polyhedra yield zeolites with slightly different structures. The aluminosilicate framework is permeated by channels which may vary in type and orientation.

As a mineral group, zeolites exist in both hydrated and dehydrated states and are typically characterized by their physical and chemical properties. For adsorption applications, the most useful zeolites are those that retain their structural integrity when dehydrated. In such a state, they have low density and may exhibit void volumes of up to 50%. Because tetrahedra or octahedra based on aluminum have a positive charge deficiency, the cations that maintain a charge balance, such as sodium or calcium, are retained in the framework structure. These cations may be exchanged, and the nature of the cation that is present

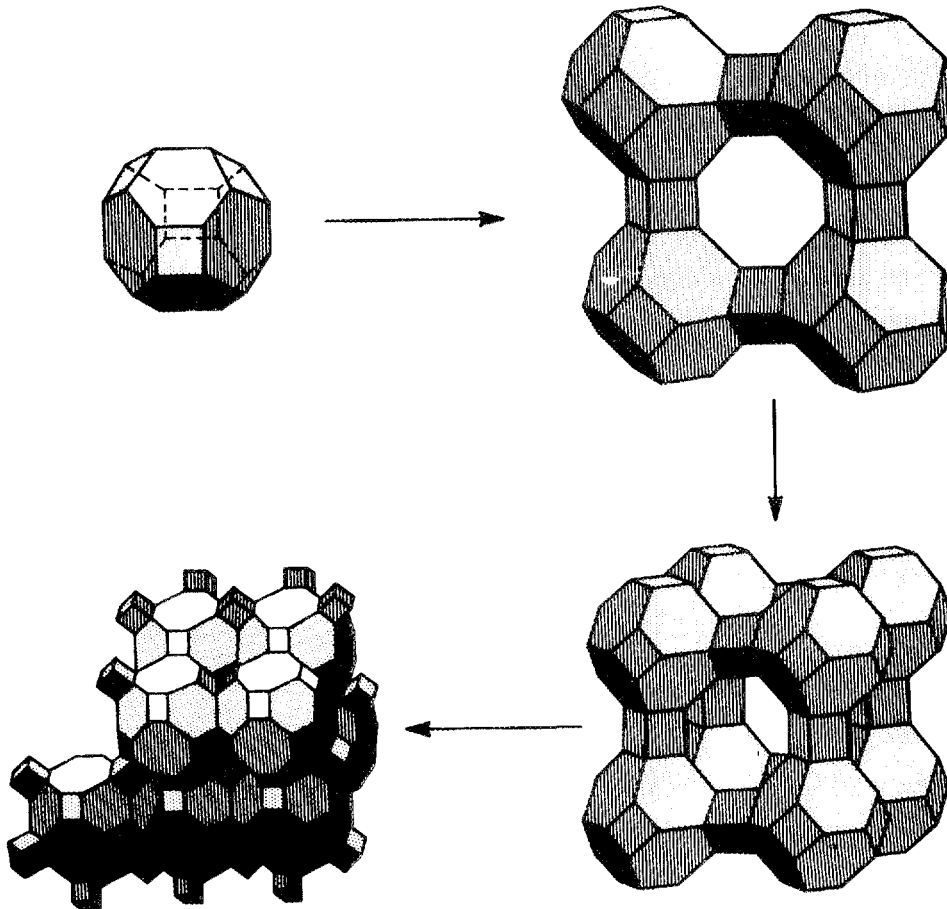
influences the physical properties of the zeolite. In particular, the retained cation influences the channel diameter and the electrical forces that determine the migration of species within the structure. Detailed information on zeolites and zeolite adsorption is found in texts by Breck (1974) and by Ruthven (1984).

The cryosorption characteristics of nitrogen ( $N_2$ ) and carbon dioxide ( $CO_2$ ) on type 4A molecular sieve are of particular interest in this study. The "4A" classification indicates a synthetic zeolite A framework structure with sodium as the major cation. A depiction of the zeolite A framework is shown in Fig. 1. Aluminum and silicon tetrahedra make up the cubic and cuboctahedral "building blocks" shown in Fig. 1a. These structures are arranged as shown to form the three-dimensional framework. Fig. 1b is a two-dimensional depiction showing the relative positions of the cuboctahedral structures and cations. The two channel structures in zeolite A are also shown. The larger channel has an aperture of  $\sim 4 \times 10^{-10}$  m and contains the  $11.2 \times 10^{-10}$ -m-diam "cage" formed by edges from four smaller cage structures. The second channel system is made up of smaller cages alternating with the larger cages, to form apertures of  $\sim 2.2 \times 10^{-10}$  m. While the relative sizes of the apertures and adsorbed molecules provide a useful indication of probable sorption behavior, other factors such as electrical interactions also influence the sorption behavior of a zeolite and a specific sorbate.

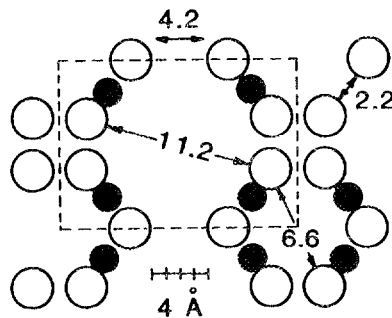
In gross form, the zeolite 4A crystals are cubic, with an edge length of  $\sim 2$   $\mu$ m, and they are pelletized using an inert clay binder that accounts for  $\sim 10\%$  of the pellet volume. Irregular macrovoids within the binder contribute potential paths for adsorption, but their overall sorption capacity is small relative to that of the channels, or microvoids, within the crystals.

While studies of the characteristics of zeolites in cryosorption pumps have been performed, the transport phenomena associated with the operation of cryopumps have not been widely studied and are not completely understood. The purpose of this study is to propose a model for the transport and adsorption of  $N_2$  and  $CO_2$  in fixed beds containing type 4A molecular sieves and to compare

ORNL DWG 86-1186



(a)



(b)

Fig. 1. Views of construction and spacing for the zeolite 4A crystalline structure.

that model with data obtained by Crabb and Perona, (1985) in experiments performed at the Oak Ridge National Laboratory (ORNL).

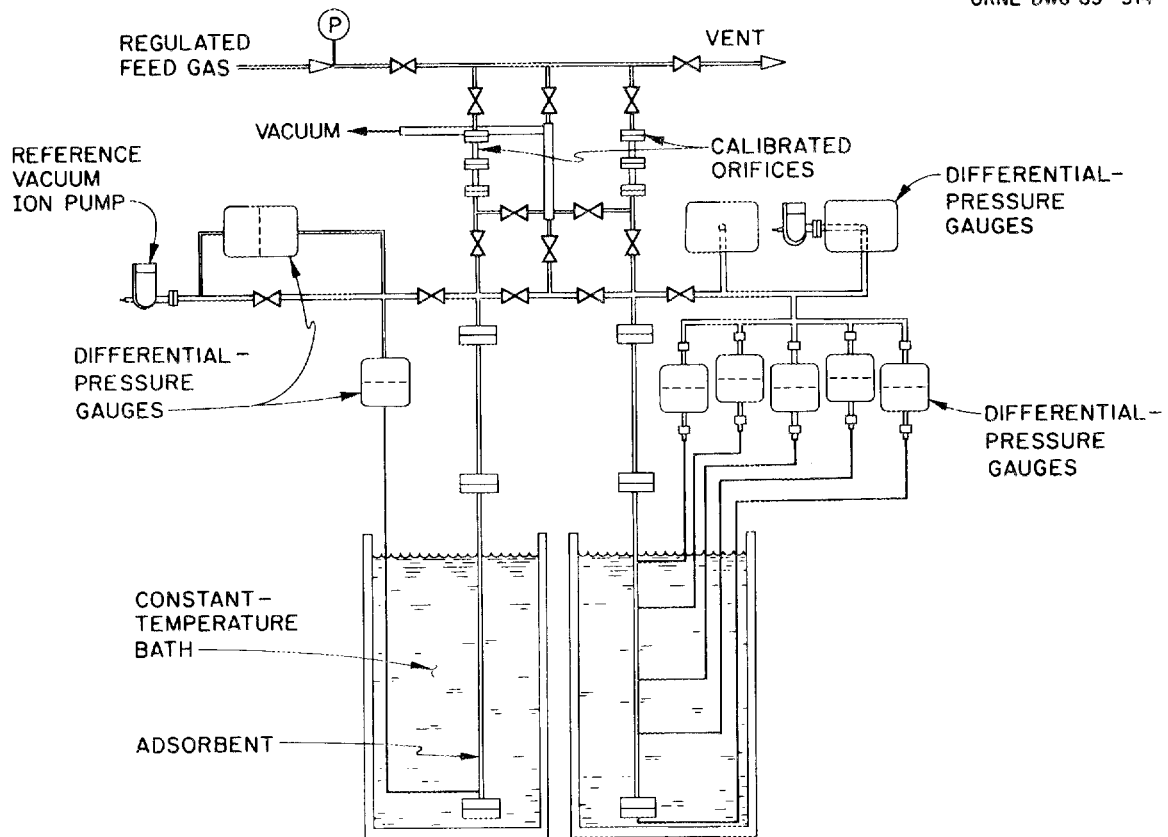
In their experiments, Crabb and Perona used the apparatus shown in Fig. 2 to adsorb  $N_2$  and  $CO_2$  on zeolite 4A molecular sieve. Their results indicate that  $CO_2$  is more strongly adsorbed on type 4A zeolite than is the  $N_2$ . To describe the sorption behavior, they also proposed a model which matched the observed behavior of  $N_2$  more closely than that of  $CO_2$ . Fig. 3 shows the data for a characteristic run using  $CO_2$ . A comparison of the initial slopes of the pressure and pressure drop curves indicates that the pressure near the bottom of the bed increased at a lower rate than the pressure at the top of the bed. The location of the peak of the pressure drop curve indicates that penetration of sorbate to the bottom of the bed was delayed for about half of the run.

Cryosorption pumping using a fixed bed of molecular sieves is a specialized application of gas adsorption in a fixed bed. Because the bed serves to collect all the adsorbed species, no flow of gas leaves the system. Therefore, unsteady-state conditions exist in the sorbent and in the bed interstices until the end of an operating cycle, at which time the sorbent is regenerated. In the application studied here, the initial pressures in the bed are sufficiently small that gas transport is in the Knudsen flow regime. As pressures in the bed become greater than 0.2 torr\*, molecular diffusion and Poiseuille flow become competing diffusive mechanisms, and it is necessary to combine their contributions to the overall pore diffusion coefficient. Operation was shown to be isothermal in the previous study (Crabb and Perona 1985).

In this study two models that describe the dynamic behavior of a sorption bed with constant gas input are considered. The first is the model proposed by Crabb et al. (1986) in studies at ORNL. Their model includes a fluid-phase mass balance (expressed as a partial differential equation) that describes the gas transport through the bed interstices as a function of position in the bed,

---

\*Units of torr are used in this paper to denote pressure, as in the previous study of Crabb et al. (1986). Such units are widely reported in the vacuum science literature.



FUNDAMENTAL PROCESSES IN SORPTION PUMPING AND TRANSFER OPERATIONS  
USING DEEP BEDS OF SORBENTS

**Fig. 2.** Apparatus used by Crabb and Perona (1985) in  $N_2$  and  $CO_2$  cryosorption experiments.

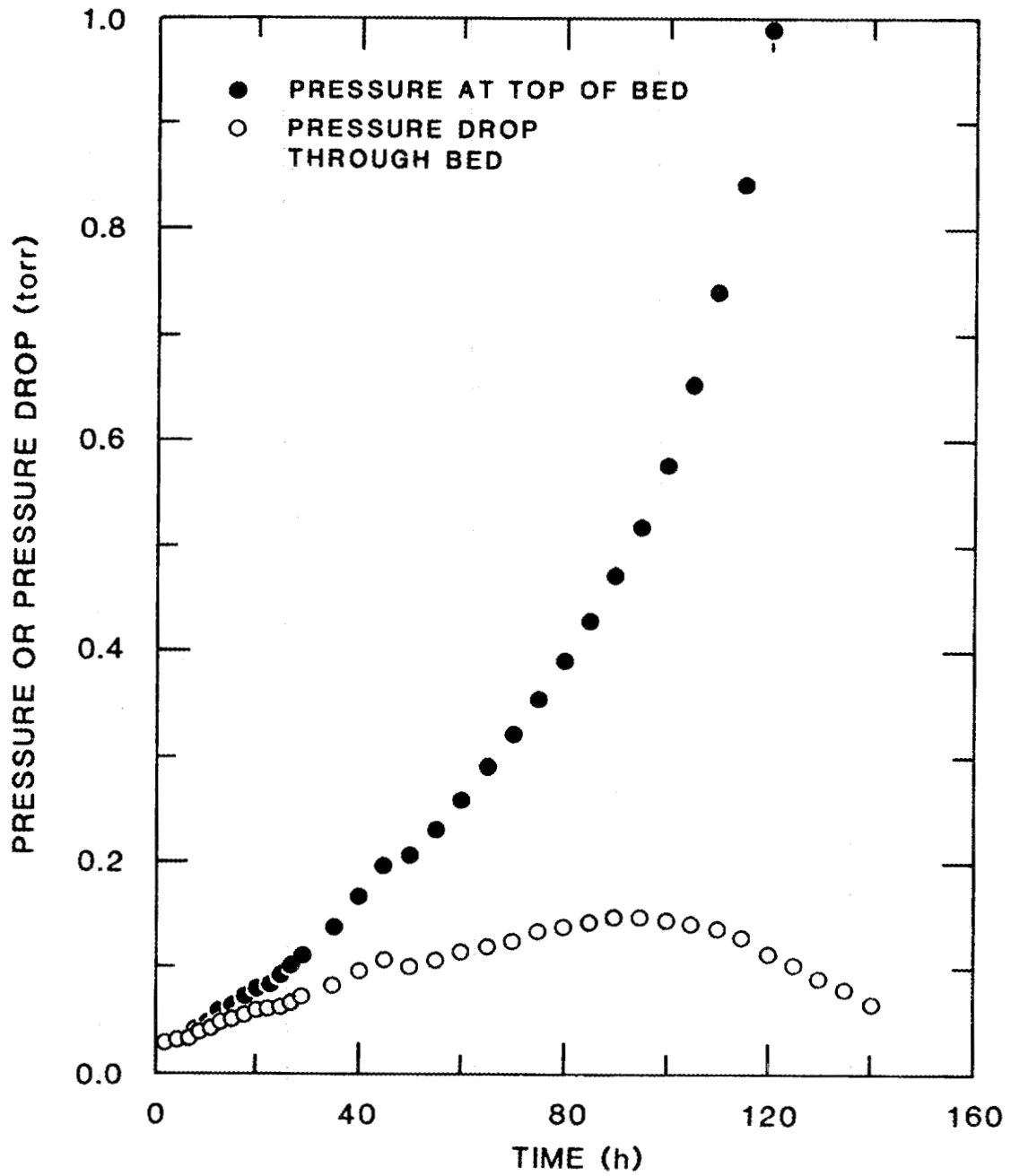


Fig. 3. Adsorption data that are typical of results obtained by Crabb and Perona in their experiments with  $\text{CO}_2$ .

coupled with an ordinary differential equation describing average sorbent (solid phase) loading in a section of the bed. The second model considered in this study includes both fluid- and solid-phase mass balances that describe the gas transport and the sorbent loading as functions of position in the bed and position in a sorbent particle. The solution of the diffusion equation and calculation of the concentration profile in the sorbent particle adds an additional level of detail to the results reported by Crabb et al. (1986). In addition, the dependence of the fluid- and solid-phase diffusivities on concentration is addressed.

Both the original Crabb model and the model developed in this study require the solution of one or more nonlinear partial differential equations. Crabb et al. (1986) employed finite differences to obtain a solution, and our proposed model uses orthogonal collocation in conjunction with a variable-order, variable-stepsize, ordinary differential equation solver. Finite-difference schemes have traditionally been a popular approach to solving equations that describe separation or reaction phenomena carried out in fixed beds (Carnahan et al, 1969; Holland and Liapis, 1983; Lapidus, 1962). They are relatively easy to program on a computer and there is an abundance of literature on their application to almost any type of problem involving partial differential equations. However, within the past 10 to 15 years, interest in the methods of weighted residuals (MWR) to solve partial differential equations has increased (Finlayson, 1972). In particular, the use of orthogonal collocation in the analysis of packed-bed reactors has been studied and reported in a number of papers and texts. In this study, orthogonal collocation is used because it offers two advantages over finite differences: relatively greater accuracy with fewer discrete points (and therefore with less computation), and a concise representation of partial derivatives as matrices, which facilitates any programming changes needed to accommodate different models.

The following section presents a more detailed examination of the literature that were helpful in understanding zeolite molecular sieves, cryosorption pumping, modeling techniques, and numerical methods. Other sections describe the

theoretical development of the models, an analysis of the theoretical results, and the relationship of these results to experimental data obtained by Crabb and Perona (1985). A summary with suggestions for additional work is presented. A detailed development of the implementation of orthogonal collocation and a partial listing of the FORTRAN computer code are given in the appendixes.

## 2. LITERATURE SURVEY

### 2.1 ZEOLITE MOLECULAR SIEVES AND CRYOSORPTION PUMPING

Zeolites were recognized as a new class of minerals in 1756 by Cronstedt, in Sweden (Breck 1974). Throughout the last half of the 1800s and the early 1900s, interest was focused on ion-exchange properties and on the reversible hydration-dehydration property of zeolites. The ability of particular dehydrated zeolites to selectively adsorb compounds was studied in the 1900s; around 1930, J.W. McBain deduced an approximate pore size for the zeolite chabazite and introduced the term "molecular sieve" (McBain 1932). In 1956, Reed and Breck of the Union Carbide Corporation described the structure of the synthetic zeolite A (Reed and Breck 1956). A complete discussion of the chemistry and use of molecular sieves is given in *Zeolite Molecular Sieves* (Breck 1974).

Since the advent of synthetic zeolites, numerous publications have addressed their applications as catalysts, ion-exchange agents, and sorbents. The use of zeolites as sorbents for gases was pioneered by R. M. Barrer, whose first publications appeared in the 1930s. His 1978 text summarizes much of the work performed on zeolites as sorbents (Barrer, 1978). Breck's text (Breck 1974) also contains an informative discussion of adsorption in zeolites.

Within the past 15 years, D. M. Ruthven and his coworkers at the University of New Brunswick have published a number of articles on the adsorption of gases in fixed beds of zeolite molecular sieves. In 1971, Ruthven and Loughlin (1971a) addressed the role of crystal shape and size distribution on diffusivities in 4A and 5A zeolite molecular sieves. Later they presented evidence that the binder used to agglomerate the zeolite crystals acts only as a diluent in the adsorption of n-butane on 5A molecular sieve, and that the controlling adsorption process occurs in the crystal microvoids (Ruthven and Loughlin 1971b). Yucel and Ruthven (1980) discussed the diffusion of CO<sub>2</sub> in 4A and 5A zeolite crystals at pressures from 8 to 200 torr and temperatures from 273 K to 371 K. Work of

the Ruthven group is summarized in his reference book on adsorption (Ruthven, 1984).

Although cryosorption pumping was first employed by Dewar around the turn of the century, active interest has increased only in recent years because of advances in cryogenic technology and the advent of research on fusion reactors. Stern and Dipaolo (1969) presented experimental results describing the adsorption of air using a cryopump with Linde 5A molecular sieve. They also included a complete bibliography of early articles describing cryosorption pumps and devices. A large portion of the work involving cryopumps and molecular sieves has been funded by governments in conjunction with energy-related programs and by manufacturers of commercially available pumps. Fisher and Watson (1976) discussed the cryosorption pumping of gaseous by-products from fusion reactors. Experiments on a cryopump designed by workers at Brookhaven National Laboratory and manufactured by Janis Research for a vacuum test facility at the Los Alamos National Laboratory were reported by Hseuh and Worwetz (1981).

Recently cryosorption pumps have found application in other processes requiring high pumping speed and a clean environment. Visser and Scheer have published several articles on pumps for various ultra-high vacuum (UHV) applications (Visser and Scheer, 1979 and 1981), including the evacuation of the process chamber in a thin-film coating process. Dennison and Gray present an interesting comparison of cryogenic and turbomolecular pumps in a commercial sputter coating process (Dennison and Gray, 1979).

## **2.2 MODELING OF ADSORPTION AND CRYOSORPTION PUMPING**

Many articles and texts have been written about the modeling of fixed beds and adsorption operations. Two texts that were useful here as general references are those by Bird, Stewart, and Lightfoot (1960) and by Holland and Liapis (1983). The latter text contains two chapters dedicated to the modeling of adsorption processes. In 1973 and 1974, Garg and Ruthven published

three papers describing different theoretical approaches to analyzing adsorption in commercial zeolite molecular sieve columns (Garg and Ruthven 1973a, 1973b, and 1974). The first two papers discuss model equations and solutions in the form of breakthrough curves for an isothermal, continuous column exposed to step change in the sorbate concentration. The third paper addresses the more general nonisothermal problem. Although the apparatus and assumptions of Garg and Ruthven differ from those of Crabb and Perona (1985), their general technique is relevant, and their discussion of the modeling implications of macropore- versus micropore-controlled diffusion were of particular interest. Of course, the work performed by Crabb et al. (1986) was the starting point for this study, and their objective was the observation and modeling of  $N_2$  and  $CO_2$  cryosorption at pressures less than or equal to 1 torr.

### 2.3 NUMERICAL METHODS

A great deal of literature is available on the use of finite-difference schemes to solve problems involving partial differential equations. Several texts emphasize problems usually associated with chemical engineering, such as the works of Carnahan, et. al. (1969) and Lapidus (1962). Another useful application-oriented text is that by Forsythe, Malcolm, and Moeller (1977). In the late 1960s and the 1970s, the application of orthogonal collocation to problems involving diffusion and reaction was introduced and researched by Villadsen and by Finlayson. Methods of weighted residuals (MWRs), in which the solution to one or more differential equations is expanded in a series of known functions with arbitrary coefficients, have been available since the 1940s. The use of one particular MWR, collocation, became popular in chemical engineering research after Villadsen and Stewart (1967) showed that solution accuracy can be enhanced if collocation points are chosen to be the roots of an orthogonal polynomial. Articles by Finlayson in the early 1970s discussed the use of orthogonal collocation in the analysis of reactions in packed beds (Finlayson, 1971; and Ferguson and

Finlayson, 1970). Later, Michelsen and Villadsen published an important paper detailing improved algorithms for calculating collocation constants (Michelsen and Villadsen, 1972). A detailed description of their work is collated in their later-published text (Michelsen and Villadsen, 1980). Finlayson has published two texts on the use of MWRs. The most recent, *Non-Linear Analysis in Chemical Engineering*, contains extensive discussions on steady-state and transient modeling of reactions using orthogonal collocation (Finlayson, 1980).

Recently, Raghavan and Ruthven (1983) have published results from an analysis of fixed-bed adsorption columns orthogonal collocation. Appendix I of their paper describes a modeling approach that serves as a precursor to the extensions developed in this investigation.

### 3. THEORY

#### 3.1 CRYOSORPTION PUMP MODEL EQUATIONS.

The primary components of the cryosorption apparatus used by Crabb and Perona are shown in Fig. 4. In their experiments the bed was evacuated and used to adsorb  $N_2$  and  $CO_2$  on approximately spherical, type 4A molecular sieve particles. The size ranges used in the experiments were 0.50–0.60 mm and 0.60–0.85 mm. The cubic, type 4A zeolite crystals, with a mean edge length of 1.7–2.0 mm, were fixed in an inert binder. However, for the purposes of this analysis, they were assumed to be spherical with volumes equal to the cube volumes. About 10% of the sieve particle volume is occupied by the binder, and the remaining volume consists of interstitial voids between the molecular sieve particles, voids within the binder (macrovoids), the solid portion of the crystal, and the intracrystal voids (microvoids).

In the experiments of Crabb and Perona (1985), gas was leaked into the head space above the bed at a controlled rate. The gas molecules diffuse into the bed through the interstices between the molecular sieve particles and into the macropores formed by the binder. In the model proposed herein, no distinction is made between the interstices and the macropores. Both are represented by a mean pore radius, which empirically describes the gas flow channel and is a factor in the calculation of the pore diffusion coefficient.

An implicit assumption in the development of this model is that the primary diffusional resistance to adsorption occurs in the crystal micropores and not in the intercrystal macropores. Consequently, the gas concentration at the crystal surface is assumed to be equal to the concentration in the bulk phase. Differences in the sorption behavior of  $N_2$  and  $CO_2$  that are apparent from the experiments performed by Crabb and Perona support the assumption of a controlling micropore resistance. They found  $CO_2$  to be much more strongly adsorbed on 4A zeolite sieves than was the  $N_2$ , for which they report diffusivities of  $\sim 10^{-25}$   $cm^2/s$  (Crabb and Perona 1985). A low affinity for  $N_2$  at low temperatures is

ORNL DWG 84-640R2

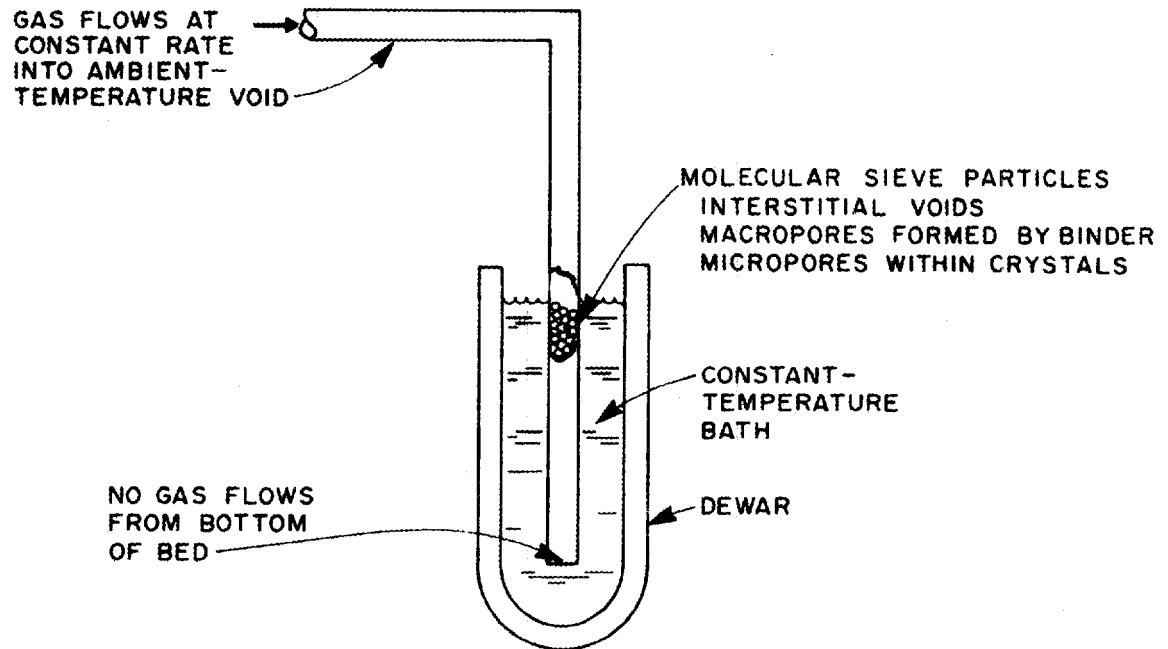


Fig. 4. Primary components of the experimental adsorption apparatus used by Crabb and Perona (1985).

described by Breck as behavior that is both anomalous and characteristic for the micropore structure of zeolite A. Because there is no basis for attributing such selective sorption behavior to the macropores in the binder, one might infer as an initial assumption that the difference in behavior between the two sorbates is due to their interaction with the microporous structure.

Crabb and Perona (1985) present a detailed development of the basic dynamic mass balance; therefore only the basic elements are discussed here. The cryosorption pump model described below is comprised of a fluid-phase mass balance that models the hydrodynamic behavior of gas flowing through the bed and a solid-phase mass balance that describes the adsorption and diffusion of the sorbate into the sorbent particle. An unsteady-state mass balance on a differential section of bed, expressed mathematically as

$$\epsilon \frac{\partial c}{\partial t} + \epsilon \frac{\partial(vc)}{\partial z} + \rho_b \frac{\partial \bar{q}}{\partial t} = 0, \quad (1)$$

relates the accumulation of sorbate within the volume in the fluid phase,  $\epsilon(\partial c/\partial t)$  the accumulation of material in the unit volume due to the changing flux of gas molecules through the interstices and macrovoids,  $\epsilon[\partial(vc)/\partial z]$ , and the mean accumulation of sorbate in the solid phase,  $\rho_b(\partial \bar{q}/\partial t)$ . The unsteady-state diffusion equation for a sphere in one dimension represents transient diffusion in the solid phase,

$$\frac{\partial q}{\partial t} = \frac{1}{r^2} \frac{\partial}{\partial r} \left[ r^2 D_z \frac{\partial q}{\partial r} \right], \quad (2)$$

where  $D_z$  is the effective zeolitic diffusivity.

Boundary conditions both at the top ( $z = 0$ ) and at the bottom ( $z = L$ ) of the bed must be considered with the fluid-phase balance. For the solid-phase balance, Eq. (2), the boundary condition at the center of the sphere is implicit in the equation, and only the concentration at the surface is required.

Because the pressure in the head space is a function of the bed behavior as well as the flow of gas into the system, an explicit boundary condition at the top of the bed is not available. The flux at the bed surface can be expressed in

terms of the flow into the system and the accumulation of gas in the head space,

$$\epsilon AD_p \left. \frac{\partial c}{\partial z} \right|_{z=0} = \frac{Q}{RT_a} - \left. \frac{\partial c}{\partial t} \right|_{h.s.} \quad (3)$$

The feed,  $Q$ , is constant. Although  $\partial c/\partial t|_{h.s.}$ , the accumulation in the head space, is not known explicitly, it can be related to the accumulation at the top of the bed. The flux at the bottom of the bed is zero, and the boundary condition at that point is expressed as

$$\left. \frac{\partial c}{\partial z} \right|_{z=L} = 0 \quad (4)$$

In considering the solid phase, the boundary condition at the surface of a sorbent crystal relates the bulk conditions in the bed to the conditions on the crystal surface. Langmuir's isotherm,

$$\frac{q(R)}{q_m} = \frac{kp}{1 + kp}, \quad (5)$$

was used by Crabb and Perona (1985) to represent the adsorption of  $\text{CO}_2$  and  $\text{N}_2$  on zeolite 4A molecular sieve. Experimental isotherm data were available for pressures as low as 1 torr, but extrapolations were necessary to include pressures experienced near the beginning of these experiments. Zero flux is assumed at the center of a sorbent crystal, or

$$\left. \frac{\partial q}{\partial r} \right|_{r=0} = 0. \quad (6)$$

The gas concentration and gas flux in Eqs. (1) and (2) can be related to experimental results most easily if they are expressed in terms of the column pressures, which are relatively simple to measure. In the experiments of Crabb and Perona, and in cryopumping systems in general, bed pressures are typically  $< 1$  torr, thus the ideal gas law may be used to define the molar gas concentration as a function of the gas pressure,

$$c = \frac{n}{V} = \frac{p}{RT}. \quad (7)$$

The gas and the solids which form the bed have been shown to be at the same constant temperature (Crabb and Perona 1985). The first term in Eq. (1), representing the accumulation of gas in the bed voids, can readily be represented in terms of the column pressure by using Eq. (7).

The second term in Eq. (1), representing the derivative of the gas flux, is more complex. Diffusion is the primary mechanism for gas flow through the bed interstices and the macrovoids in the sieve particles. The flux of gas molecules through a cross-section of the bed can be represented using a form of Fick's law with an effective pore diffusivity,  $D_p$ :

$$\frac{\partial(vc)}{\partial z} = D_p \frac{\partial^2 c}{\partial z^2} \quad (8)$$

Crabb et al. (1986) suggest that Knudsen diffusion, characterized by a molecular mean free path that is larger than the flow channel, is the primary diffusive mechanism at pressures of interest in their experiments. Ruthven (1984) suggests the following equation for estimating  $D_K$ , the Knudsen diffusivity:

$$D_K = 9700 r_p \left( \frac{T}{M} \right)^{0.5}, \quad (9)$$

where  $r_p$  is the mean pore radius (cm) and  $M$  is the molecular weight of the diffusing species. If the gas molecules are assumed to be non-interacting rigid spheres, the mean free path can be computed as a direct function of temperature and an inverse function of pressure,

$$\lambda = \frac{k_B T}{(2\pi d^2 p)^{0.5}}. \quad (10)$$

The mean free paths of CO<sub>2</sub> molecules at 198 K range from 2.2 mm at 0.01 torr to 0.022 mm at 1.0 torr. Estimates of a mean flow channel diameter can be made based on assumptions about the particle shape and packing geometry. Crabb and Perona (1985) estimate a hydraulic diameter of  $\sim 0.064$  mm. In the higher-pressure regions that begin to prevail as the bed becomes saturated, the

molecular mean free path appears to be approximately equal to or smaller than the hydraulic diameter of the flow channels. Under these conditions, molecular diffusion, characterized by a mean free path that is smaller than the flow channel, and Poiseuille flow may become competing diffusive mechanisms. The molecular diffusivity can be estimated from the Chapman-Enskog equation (Bird, Stewart, and Lightfoot, 1960) modified for a diffusing species that is an ideal gas,

$$D_m = 0.001858 \frac{\sqrt{\frac{2T^3}{M}}}{p\sigma^2\Omega}, \quad (11)$$

where  $\sigma$  and  $\Omega$  are Lennard-Jones parameters. Ruthven (1984) gives the following equation for estimating the contribution of Poiseuille flow to the gas diffusivity:

$$D_{\text{Pois}} = \frac{pr_p}{8\mu}, \quad (12)$$

where  $\mu$  is the gas viscosity (g-cm/s), which can be calculated from

$$\mu = 2.6693 \times 10^{-5} \frac{\sqrt{M \cdot T}}{\sigma^2\Omega}. \quad (13)$$

Eq. (13) is from Bird, Stewart, and Lightfoot (1960). For a system involving a gas in which the temperature is constant, Eqs. (9), (10), and (12) reduce to functions of the pore radius,  $r_p$ , and the gas pressure,  $p$ . Ruthven (1984) gives the following equation for estimating the pore diffusivity from the component diffusivities described above:

$$D_p = \left[ \frac{1}{D_K} + \frac{1}{D_m} \right]^{-1} + D_{\text{Pois}}. \quad (14)$$

At low pressures and small pore radii, collisions of molecules with the walls of pores are the primary resistance to flow, and Knudsen diffusion is dominant. At higher pressures when collisions between molecules become the primary resistance to flow, molecular diffusion and Poiseuille flow are dominant. In the transition region, contributions from all three mechanisms may be computed using Eq. (14).

In the solid phase, the diffusivity of the sorbate within the crystals is also considered to be dependent on the concentration of the diffusing species. Garg and Ruthven (1973a) suggest that the Darken equation,

$$D_z = D_0 \left[ \frac{\partial(\ln p)}{\partial(\ln q)} \right], \quad (15)$$

which was originally derived for the interdiffusion of two alloys, be used to represent the zeolitic diffusivity. Ruthven (1984) refers to  $D_0$  as the corrected diffusivity, and suggests that diffusion in activated zeolitic structures resembles the interdiffusion of alloys for which the Darken equation was derived. In such a case, if the Langmuir relationship describes the equilibrium between the gas and solid phases, then the derivative in Eq. (15) can be computed to be

$$D_z = \frac{D_0}{\left(1 - \frac{q}{q_m}\right)}. \quad (16)$$

Incorporating the concentration-dependent diffusivity, the diffusion equation for the sorbent particle can be rewritten as

$$\frac{\partial q}{\partial t} = \frac{1}{r^2} \frac{\partial}{\partial r} \left[ r^2 D_z(q) \frac{\partial q}{\partial r} \right]. \quad (17)$$

Returning to Eq. (1), it will not be possible to express the average accumulation of the sorbate in the solid phase,  $\rho_b(\partial\bar{q}/\partial t)$ , as a simple function of the pressure. However, it can be expressed in terms of the other dependent variable, the point solid loading,  $q$ . The concentration profile can be integrated to obtain  $\bar{q}$ , and  $\partial\bar{q}/\partial t$  can be computed by difference, but it is numerically complex to do so. Instead,  $\partial\bar{q}/\partial t$  can be calculated in terms of the sorbate flux at the surface of the crystal. Because the net flux in a crystal is assumed to be inward, a crystal acts as a mass sink, and the flux of sorbate across the crystal surface is equivalent to the instantaneous mean accumulation in the crystal. The accumulation

can be calculated from the concentration gradient at the crystal surface and the packing characteristics of the sorbent:

$$\frac{\partial \bar{q}}{\partial t} = D_z(q) \phi_z \left. \frac{\partial q}{\partial r} \right|_{r=R}, \quad (18)$$

where  $\phi_z$  is the crystal surface area per unit crystal volume, or  $3/R$ .

Incorporation of Eqs. (15) through (18) into the model Eqs., (1) and (2), with boundary conditions given by Eqs. (3) through (6), yields the fluid and solid balances in terms of the gas pressure and the solid loading. The fluid-phase balance, with boundary conditions at the top and bottom of the bed is expressed as:

$$\left. \frac{\partial p}{\partial t} \right|_z = \frac{RT}{\epsilon} \left\{ \frac{\epsilon D_p(p)}{RT} \frac{\partial^2 p}{\partial z^2} - \rho_b \left[ D_z(q) \phi_z \left. \frac{\partial q}{\partial r} \right|_{r=R} \right] \right\}, \quad (19)$$

$$\left. \frac{\partial p}{\partial z} \right|_{z=0} = \frac{RT}{\epsilon A D_p(p)} \left[ \frac{V}{RT_a} \left. \frac{\partial p}{\partial t} \right|_{h_s} - \frac{Q}{RT_a} \right], \quad (20)$$

and

$$\left. \frac{\partial p}{\partial z} \right|_{z=L} = 0. \quad (21)$$

The solid-phase balance is given by:

$$\frac{\partial q}{\partial t} = \frac{1}{r^2} \frac{\partial}{\partial r} \left[ r^2 D_z(q) \frac{\partial q}{\partial r} \right]. \quad (22)$$

with boundary conditions at the surface,

$$q(R) = \frac{q_m k p}{1 + k p}, \quad (23)$$

and in the center,

$$\left. \frac{\partial q}{\partial r} \right|_{r=0} = 0. \quad (24)$$

### 3.2 NUMERICAL SOLUTION

Eqs. (19) and (22) are parabolic, nonlinear partial differential equations (PDE) that are coupled by conditions at the surface of the sorbent crystal. In physical terms, diffusion through the bed and diffusion in the solid are interacting phenomena, and the interaction occurs at the crystal surface. Because the only source of gas is at the bed entrance, concentration profiles in both phases asymptotically approach saturation.

The pressure,  $p$ , solid-loading,  $q$ , axial distance,  $z$ , and radial distance,  $r$ , in Eqs. (19) and (22) can be made dimensionless using

$$\begin{aligned}\hat{p} &= \frac{p(z, t)}{p_r}, & \hat{q} &= \frac{q(z, r, t)}{q_m}, \\ \hat{z} &= \frac{z}{L}, & \hat{r} &= \frac{r}{R}.\end{aligned}\tag{25}$$

In terms of the dimensionless variables, Eqs. (19) through (24) are rewritten as

$$\frac{\partial \hat{p}}{\partial t} = \frac{RT}{\epsilon p_r} \left\{ \frac{\epsilon D_p(\hat{p}) p_r}{RTL^2} \frac{\partial^2 \hat{p}}{\partial \hat{z}^2} - \rho_b \left[ D_z(\hat{q}) \phi_z \frac{q_m}{R} \frac{\partial \hat{q}}{\partial \hat{r}} \Big|_{\hat{r}=1} \right] \right\}, \tag{26}$$

$$\frac{\partial \hat{p}}{\partial \hat{z}} \Big|_{\hat{z}=0} = \frac{RTL}{\epsilon AD_p(\hat{p}) p_r} \left[ \frac{V p_r}{RT} \frac{\partial \hat{p}}{\partial t} \Big|_{h_s} - \frac{Q}{RT_a} \right], \tag{27}$$

$$\frac{\partial \hat{p}}{\partial \hat{z}} \Big|_{\hat{z}=1} = 0, \tag{28}$$

and

$$\frac{\partial \hat{q}}{\partial t} = \frac{1}{(R\hat{r})^2} \frac{\partial}{\partial \hat{r}} \left[ \hat{r}^2 D_z(\hat{q}) \frac{\partial \hat{q}}{\partial \hat{r}} \right], \tag{29}$$

$$\hat{q}(\hat{r} = 1) = \frac{k p_r \hat{p}}{1 + k p_r \hat{p}}, \tag{30}$$

$$\left. \frac{\partial \hat{q}}{\partial \hat{r}} \right|_{\hat{r}=0} = 0. \quad (31)$$

Representation of Eqs. (26) through (31) in a form amenable to a numerical solution using orthogonal collocation requires (1) representation of the spatial derivatives at each time step using orthogonal collocation, and (2) solution of the resulting set of time-dependent ordinary differential equations.

### 3.3 APPLICATION OF ORTHOGONAL COLLOCATION.

The collocation method is one of a broader class of MWRs in which a function containing unknown, arbitrary coefficients is introduced as a trial solution to a differential equation. The coefficients are computed to give the best fit to the differential equation according to several possible criteria. In the collocation method, the trial function is forced to fit the differential equation at predetermined discrete points. The solution at those points is computed by solving  $N$  simultaneous algebraic equations that result from the substitution of the trial function into the differential equation, where  $N$  is the number of arbitrary constants in the trial function. Villadsen and Stewart (1967) established that collocation points chosen to be roots of Jacobi orthogonal polynomials are optimal, in the sense that they maximize the order of the solution approximation. In the cryosorption pump model, a polynomial approximation is used, and a discrete solution is obtained for spatial derivatives of  $\hat{p}$  and  $\hat{q}$ . As a result of the polynomial approximation, the right hand sides of Eqs. (26) and (29) are expressed as algebraic functions of  $\hat{p}$  and  $\hat{q}$ , and the model is transformed into a set of ordinary differential equations.

The Jacobi polynomial trial functions for  $\hat{p}$  and  $\hat{q}$  can be expressed as

$$\hat{p}_{N+2}(\hat{z}, t) = (1 - \hat{z})\hat{p}(0, t) + \hat{z}\hat{p}(1, t) + \hat{z}(1 - \hat{z}) \sum_{i=1}^N c_i(t) J_i(\hat{z}), \quad (32)$$

and

$$\hat{q}_{M+1}(\hat{z}, \hat{r}, t) = \hat{q}(\hat{z}, 1, t) + (1 - \hat{r}) \sum_{i=1}^M d_i(t) J_i(\hat{r}), \quad (33)$$

where the polynomials  $J_i(x)$  are defined by

$$\int_0^1 W(x) J_i(x) J_j(x) dx = 0, \quad (j \neq i; j = 0, \dots, i-1), \quad (34)$$

with  $W(x) = x^\beta (1-x)^\alpha$ . Eq. (32) represents  $N$  interior collocation points and two points at the boundaries of the bed. Eq. (33) represents  $M$  points through the interior of the sphere and one boundary point at the surface. The boundary condition at the center of the sphere is implicit in the model formulation and is not represented by the trial solution. Eq. (34) is a frequently used representation of the Jacobi polynomials, but more practical recursive methods are typically used to find polynomial coefficients. They are described briefly, along with a more detailed mathematical description, in Appendix A.

Equations (32) and (33) are effectively perturbations of the boundary conditions on the fluid- and solid-phase balances [Eqs. (26) and (29)]. If the trial functions were substituted directly into the equations, one possible result would be a set of  $(N+2) \times (M+1)$  ordinary differential equations and  $(N+2)$  algebraic equations (the solid loading at the crystal surface defined by the equilibrium adsorption isotherm), with the same number of arbitrary constants. One equation would correspond to each collocation point, and the equations could be solved simultaneously for the arbitrary constants. Villadsen and Stewart (1967) describe a method in which the equations are solved in terms of discrete solution values at the collocation points instead of polynomial coefficients. Their approach yields the following compact expressions for the spatial derivatives:

$$\frac{\partial \hat{p}_i}{\partial \hat{z}} = (\overline{AG}) \hat{p} = \sum_{j=1}^{N+2} AG_{i,j} \hat{p}_j, \quad (35)$$

$$\frac{\partial^2 \hat{p}_i}{\partial \hat{z}^2} = [(\overline{AG})(\overline{AG})] \hat{p} = \sum_{j=1}^{N+2} AG_{i,j} \left[ \sum_{k=1}^{N+2} AG_{j,k} \hat{p}_k \right], \quad (36)$$

$$\frac{\partial \hat{q}_{i,j}}{\partial \hat{r}} = (\overline{AS}) \hat{q} = \sum_{j=1}^{M+1} AS_{i,j} \hat{q}_j, \quad (37)$$

$$\frac{\partial^2 \hat{q}_{i,j}}{\partial \hat{r}^2} = [(\overline{AS})(\overline{AS})] \hat{q} = \sum_{j=1}^{M+1} AS_{i,j} \left[ \sum_{k=1}^{M+1} AS_{j,k} \hat{q}_k \right]. \quad (38)$$

$\overline{AG}$  and  $\overline{AS}$  are referred to by Michelsen and Villadsen (1978) as discretization matrices. They are effectively differential operators for  $\hat{p}$  and  $\hat{q}$ , the dimensionless pressure and solid-loading solution vectors.

Using the notation shown in Eqs. (35) through (38), the boundary conditions on the fluid-phase balance at the top and bottom of the bed can be represented as,

$$\left. \frac{\partial \hat{p}}{\partial \hat{z}} \right|_{\hat{z}=0} = \sum_{j=1}^{N+2} AG_{1,j} \hat{p}_j = \frac{RTL}{\epsilon AD_p(\hat{p})p_r} \left( \frac{Q}{RT_a} + \frac{V}{RT} \left. \frac{\partial \hat{p}}{\partial t} \right|_{h_s} \right), \quad (39)$$

$$\left. \frac{\partial \hat{p}_i}{\partial \hat{z}} \right|_{\hat{z}=1} = \sum_{j=1}^{N+2} AG_{N+2,j} \hat{p}_j = 0. \quad (40)$$

The boundary condition at the surface of the sorbent does not contain derivatives. The interior condition is

$$\left. \frac{\partial \hat{q}}{\partial \hat{r}} \right|_{\hat{r}=0} = \sum_{j=1}^{M+2} AS_{1,j} \hat{q}_j = 0, \quad (41)$$

but this does not appear explicitly in the model equations. With the boundary conditions incorporated, the model equations are:

$$\begin{aligned} \frac{\partial \hat{p}_1}{\partial t} = & \left[ 1 - \frac{RT_b}{\epsilon p_r} \frac{\epsilon D_p(\hat{p})p_r}{RT_b L^2} \frac{RT_b L}{\epsilon AD_p(\hat{p})p_r} \frac{V p_r}{RT_a} AG_{1,1} \right]^{-1} \times \\ & \left\{ \frac{RT_b}{\epsilon p_r} \left[ \frac{\epsilon D_p(\hat{p})p_r}{RT_b L^2} \left[ \sum_{j=2}^{N+1} AG_{i,j} \left( \sum_{k=1}^{N+2} AG_{j,k} \hat{p}_k \right) - AG_{1,1} \frac{RT_b L}{\epsilon AD_p(\hat{p})p_r} \frac{Q}{RT_a} \right] \right. \right. \\ & \left. \left. - \rho_b \left( D_z(\hat{q}) \phi_z \frac{q_m}{R} \sum_{j=1}^{M+1} AS_{M+1,j} \hat{q}_j \right) \right] \right\}; \quad (42) \end{aligned}$$

Fluid Phase (Interior of Bed)

$$\frac{d\hat{p}_i}{dt} = \frac{RT_b}{\epsilon p_r} \left\{ \frac{\epsilon D_p(\hat{p})}{RT_b L^2} \left[ \sum_{j=2}^{N+1} AG_{i,j} \left( \sum_{k=1}^{N+2} AG_{j,k} \hat{p}_k \right) \right. \right. \\ \left. \left. - AG_{1,1} \frac{RT_b L}{\epsilon AD_p(\hat{p}) p_r} \left( \frac{V p_r}{RT_a} \frac{d\hat{p}_1}{dt} - \frac{Q}{RT_a} \right) \right] \right. \\ \left. - \rho_b \left( D_z(\hat{q}) \phi_z \frac{q_m}{R} \sum_{j=1}^{M+1} AS_{M+1,j} \hat{q}_j \right) \right\}. \quad (43)$$

Solid Phase (Surface of Sorbent Particle)

$$\hat{q}(\hat{r} = 1) = \frac{k p_r \hat{p}}{1 + k p_r \hat{p}}; \quad (44)$$

Solid Phase (Interior of Sorbent Particle)

$$\frac{d\hat{q}_{i,j}}{dt} = \frac{1}{(R\hat{r}_j)^2} \left[ \sum_{k=1}^{M+1} D_z(\hat{q}_{i,k}) \hat{r}_k^2 AS_{j,k} \left( \sum_{h=1}^{M+1} AS_{k,h} \hat{q}_{i,h} \right) \right], \quad (45)$$

where  $i = 1, \dots, M$ .

### 3.4 SOLUTION OF THE MODEL EQUATIONS

Equation (42) applies only to the collocation point at the top of the column. Equation (43) is written for the (N+1) remaining fluid-phase points. For each point in the fluid phase, the concentration profile in the solid phase is represented by (M+1) collocation points, with (M) corresponding to the discretized diffusion equation representing the interior of the sphere. The remaining point corresponds to the crystal surface, for which the value of the dependent variable,  $q$ , is defined by Langmuir's isotherm. As a group, Eqs. (42) through (45) comprise  $(N+2) \times (M+1)$  simultaneous ordinary differential equations and  $(N+2)$  algebraic equations.

The Livermore Solver for Ordinary Differential Equations (LSODE) was used to integrate the set defined by Eqs. (42) through (45). The LSODE employs Gear's method, a variable-stepsize, variable-order, predictor-corrector technique that is suitable for stiff equations. Widely varying zeolitic diffusivities, like those exhibited by  $N_2$  and  $CO_2$ , affect the sorption dynamics and contribute to varying degrees of stiffness.

Theoretical results (described in Sec. 4) were computed using 4 interior collocation points for the bed (6 total points, including the boundary points) and using 3 interior points for the sorbent particle (4 total points, including the surface). Solution accuracy, in terms of the pressure at the top of the bed and the pressure drop, was not improved by further increasing the number of collocation points. Figure 5 shows the small differences in the pressure and pressure drop curves obtained using 1, 4, and 8 interior bed points for a typical  $CO_2$  run. In general, changes in the number of collocation points for the solid phase do not significantly affect the pressure and pressure drop curves. However, erratic results for concentrations near the center of the spheres are typical for early times in the run when concentrations in some parts of the bed are near zero.

A noteworthy characteristic of the curves shown in Fig. 5 is their "jagged" appearance. The apparent discontinuities in the curve correspond to integration stepsize changes and are welcome evidence that the integrator is maintaining the solution within specified tolerances. For the sake of appearance, the curves are smoothed in subsequent figures.

Our computations of the discretization matrices and zeros of the Jacobi polynomials were modeled after subroutines published by Michelsen and Villadsen (1982). Initial conditions for the pressure and solids loading were assumed to be zero, and calculations were continued only to the point when the pressure at the top of the bed reached 1 torr.

As described earlier, the boundary condition on the fluid-phase mass balance at the top of the bed is problematic because it contains two terms ( $\partial p / \partial t|_{h_s}$  and  $\partial p / \partial z|_{z=0}$ ), that are dependent on the behavior of the bed. The second term,

ORNL DWG 86-1241

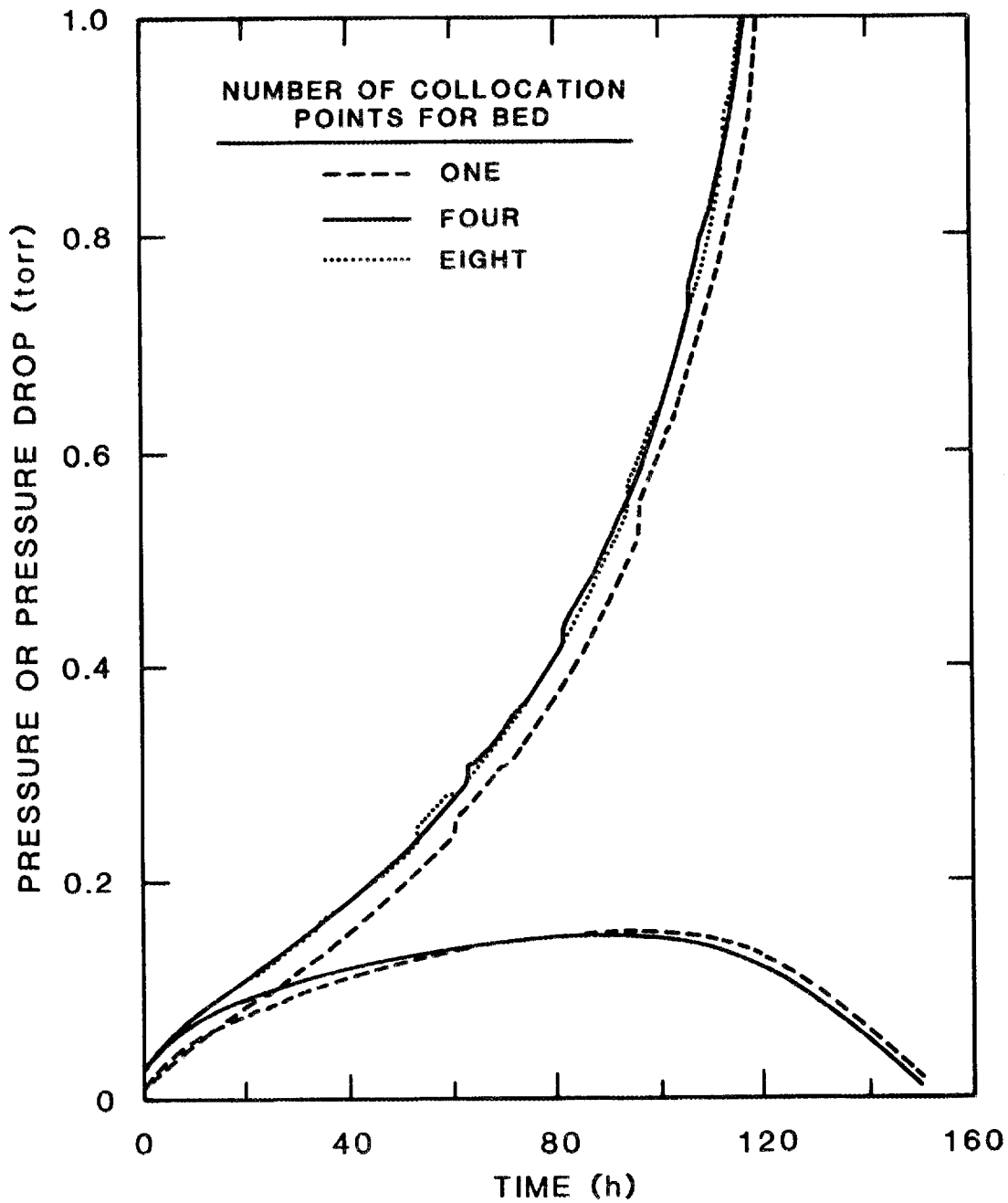


Fig. 5. The effect of the number of bed collocation points on the computed solution for a typical  $\text{CO}_2$  run of Crabb and Perona (1985).

$\partial p/\partial z|_{z=0}$ , is resolved by incorporating it into the expression for  $\partial^2 p/\partial z^2|_{z=0}$ , however,  $\partial p/\partial t|_{h_s}$  is left undefined. Physically,  $\partial p/\partial t|_{h_s}$  represents the pressure increase in the head space above the bed. The head space can be considered a separate control volume that interacts with the bed, in which case the flux at the interface of the control volumes must be computed iteratively, involving undesirable additional computation. An alternate approach taken here involves the assumption that the pressure in the head space closely follows the pressure at the top of the bed for most of an adsorption run. Similarly, the time-derivatives of the two pressure should be nearly equal. Such an assumption can be used to equate  $\partial p/\partial t|_{z=0}$  and  $\partial p/\partial t|_{h_s}$ , and to eliminate  $\partial p/\partial t|_{h_s}$  from the boundary condition. As a result, the fluid-phase balance at the top of the bed must be rearranged so that  $\partial p/\partial t|_{z=0}$  appears only on the left side of the equation, as shown in Eq. (42).

## 4. RESULTS

### 4.1 ORTHOGONAL COLLOCATION WITH THE MODEL OF CRABB AND PERONA

The model proposed by Crabb et al. (1986) employs a fluid-phase mass balance similar to that of Eq. (19), with boundary conditions equivalent to those shown in Eqs. (20) and (21). For the solid phase, they assume a parabolic concentration profile in the molecular sieve particle and reduce the partial differential equation given by Eq. (26) to an ordinary differential equation of the form

$$\frac{d\bar{q}}{dt} = \frac{15D}{R^2} [f(p) - \bar{q}] , \quad (46)$$

where the diffusivity,  $D$ , is constant, and  $f(p)$  is the Langmuir adsorption isotherm equation. The fluid-phase balance and Eq. (46) were solved using finite differences.

Crabb and Perona (1986) reported comparisons of computed and observed results from seven experiments with  $N_2$  and from four with  $CO_2$ . Their adsorption data are expressed in terms of the pressure at the top of the bed and the pressure drop through the bed. Figs. 6 and 7 are typical of their theoretical and experimental results for  $N_2$  and  $CO_2$ , respectively. The different time scales for the pressure curves emphasize the different sorption rates of the gases. The pressure of  $N_2$  above the bed is characterized by a period of gradual, nearly linear increase – clearly distinguished from a final sharp pressure increase. The pressure drop through the bed tracks the gradual pressure increase at the top of the bed and then decreases sharply, in correspondence with the sharp increase in the pressure above the bed, indicating gas penetration of the bed. The model-predicted results for  $N_2$ , shown as the solid curves in Fig. 6, agree well during the period of near-linear increase, but do not accurately predict the turning point in the curves or the ultimate slope of the rise in pressure above the bed. The  $CO_2$  data of Fig. 7 indicate that the pressure above the bed rises nonlinearly and that, unlike the  $N_2$  pressure, the pressure drop is not coincident with the

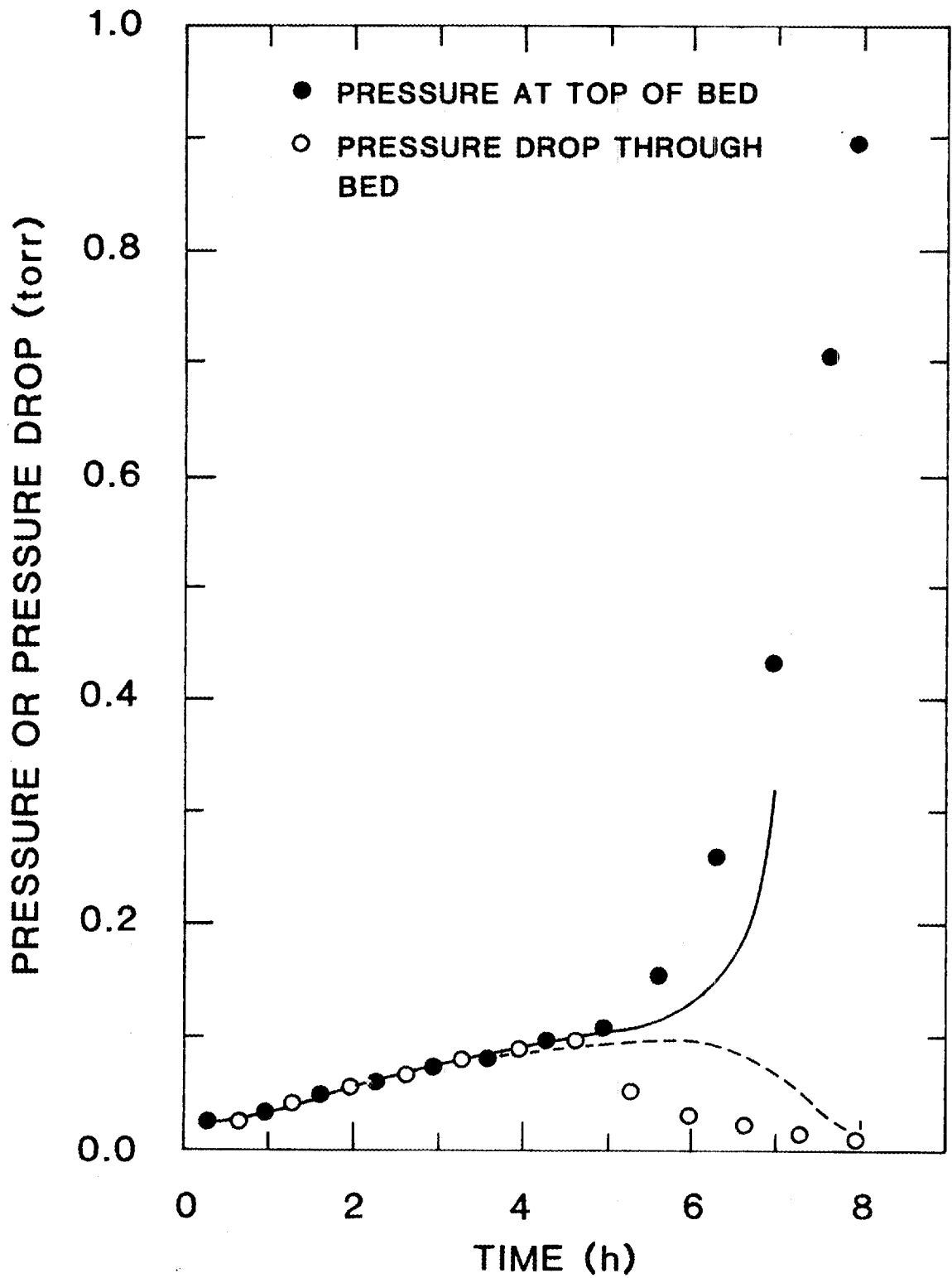


Fig. 6. Predicted vs. Observed results for  $N_2$  reported by Crabb and Perona (1985) for Run 208.

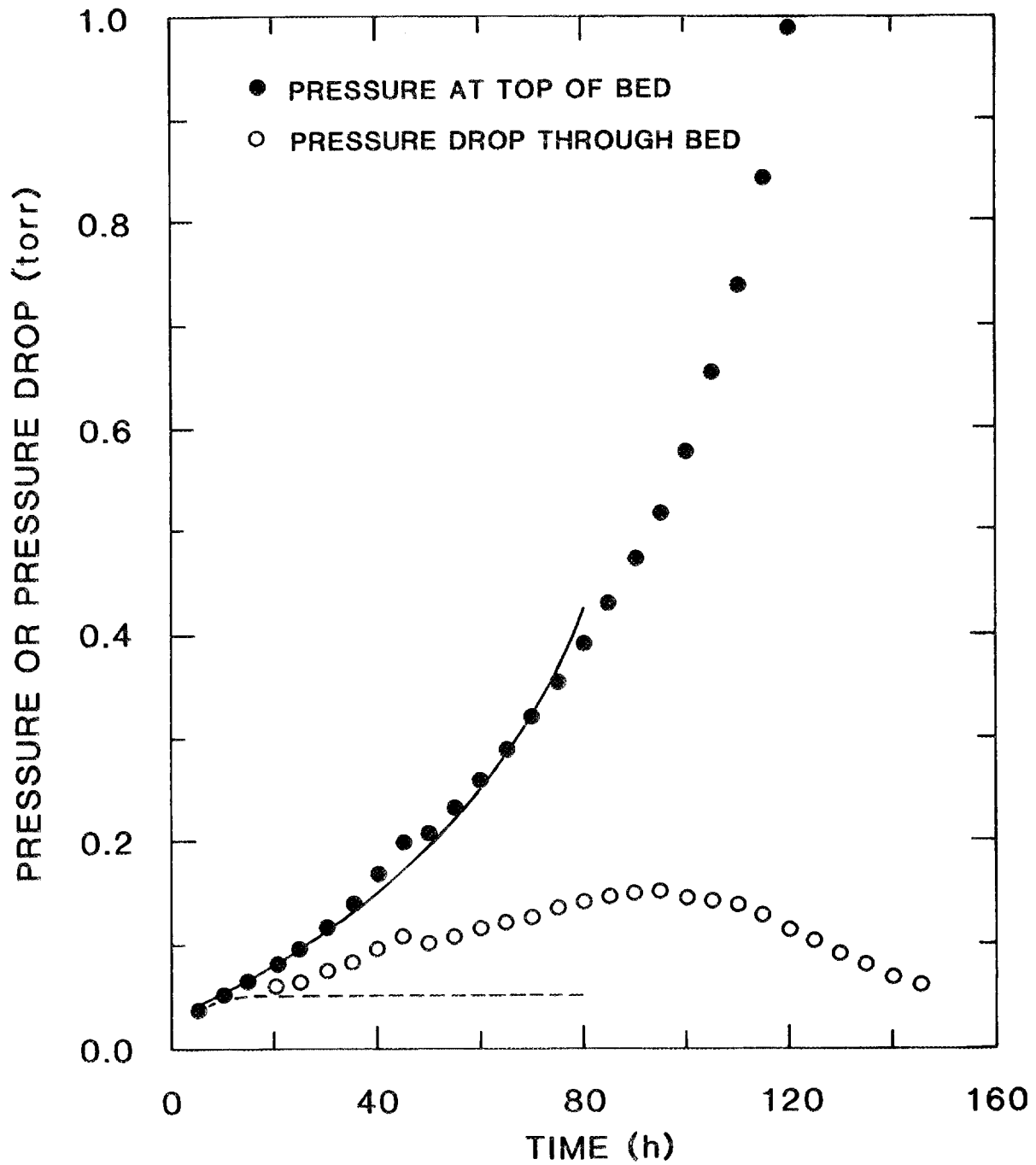


Fig. 7. Predicted vs. Observed results for  $\text{CO}_2$  reported by Crabb and Perona (1985) for Run 218.

pressure above the bed. The predicted pressure above the bed agrees with data for the early part of the run but appears to increase more sharply when the pressure reaches  $\sim 0.5$  torr. In addition, the predicted pressure drop curve lacks the increasing and decreasing pattern that is typical of the experimental results.

The feasibility of this work was demonstrated by its duplication of the theoretical results given by Crabb and Perona, using the orthogonal collocation method with their model. Orthogonal collocation was used because it has been successfully applied by researchers to similar problems (Finlayson, 1971 and 1980; Raghavan and Ruthven, 1983), because derivatives can be concisely represented and manipulated to accommodate different models, and because relatively high accuracy can be attained without excessive computational effort. An example of the match between solutions obtained via both techniques is shown in Fig. 8. Five collocation points produced results comparable to those obtained by Crabb and Perona using 10 finite-difference intervals. The time required for the solution using orthogonal collocation was approximately 50 times less than that required using finite differences. As Fig. 7 shows, the differences between the solutions are small and are within the limits of experimental error assignable to the actual results.

Some flexibility in modeling the boundary condition at the top of the bed was sacrificed by the use of orthogonal collocation. The derivative of pressure with respect to axial distance,  $\partial p/\partial z$ , at the top of the bed is easily formulated in terms of finite differences,

$$\left. \frac{\partial p}{\partial z} \right|_{z=0} \approx \frac{p(\text{head space}) - p(\text{top of bed})}{z_0 - z_1} \quad (47)$$

Because the first and last collocation points are chosen to correspond with boundary conditions in the bed, such a formulation across the boundary at the bed surface is not easily accomplished using orthogonal collocation. This difficulty was circumvented by making the assumption already discussed, that the time-derivative of the pressure in the head space is equal to the time-derivative of the pressure at the top of the bed.

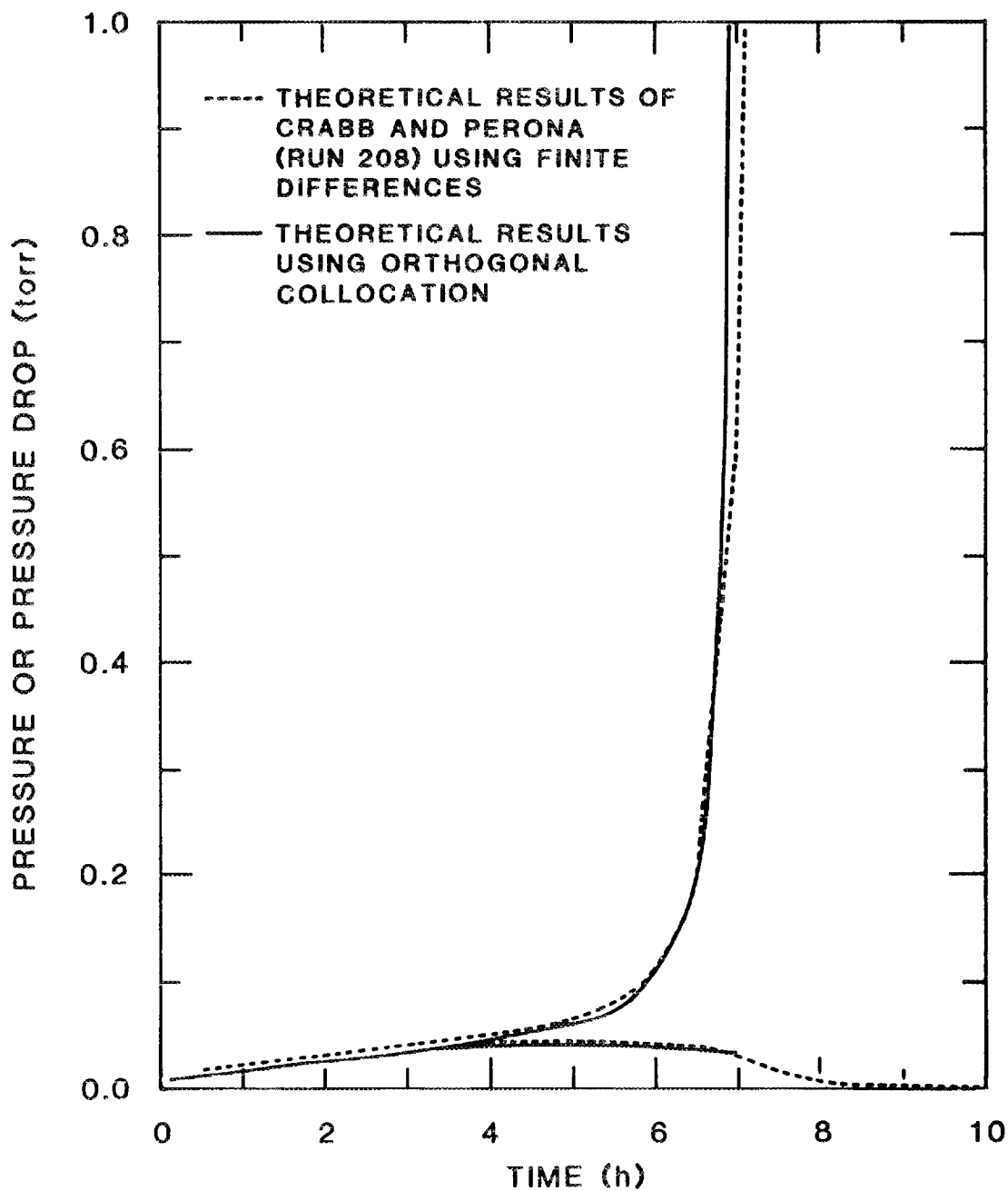


Fig. 8. Comparison of finite-difference and orthogonal collocation solutions to the model of Crabb and Perona (1985) for Run 208 with  $N_2$ .

## 4.2 COMPARISON OF PROPOSED MODEL AND EXPERIMENTAL RESULTS

Selected experimental results of Crabb and Perona (1985) and numerical results from the solution of Eqs. (23) through (26) are the basis for the comparisons discussed in this section. All four CO<sub>2</sub> runs and three of the seven N<sub>2</sub> runs made by Crabb and Perona are examined. The experimenters varied the molecular sieve particle size, the bed depth, and the gas feed rate. Table 1 summarizes the relevant experimental conditions.

Table 2 lists constants and parameters used in initial comparisons of theoretical and experimental results. Physical characteristics of the experimental system, such as the bed cross-sectional area, depth of the bed, bed temperature, sorbate feed rate, ambient temperature, volume of head space above the bed, and the bulk density of the bed, are provided by Crabb and Perona and are assumed to be constants in calculations performed using the model. The zeolite crystal density is given by Breck (1974). The effective crystal radius was calculated from data taken by Crabb and Perona, although Type 4A zeolite crystals are in fact cubic and are not uniform in size. Crabb and Perona report a size distribution that is approximately normal, with a mean edge length of 1.86  $\mu\text{m}$ . For the purposes of this study, crystals are assumed to be spherical, with a radius such that the sphere volume is equal to the mean cubic volume. Crabb and Perona also performed calculations to estimate the mean pore radius for gas flow within the bed. Their calculations were based on the assumptions that spherically shaped molecular sieve particles, and not zeolite crystals, are the primary diffusional resistance to adsorption and that bulk flow takes place only within the interstitial voids between molecular sieve particles.

Our analysis presented here is based on different assumptions, but the mean pore radius in such complex media is generally applicable as an empirical parameter that represents the average size of the gas flow path. The fraction of bed volume occupied by zeolite crystals and the fraction of bed volume available to the gas were estimated from data given by Breck in the final chapter of

**Table 1: Experimental runs of Crabb and Perona analyzed in this study**

Run	Sorbate	Mol. sieve $d_p$ (cm)	Bed height (cm)	Bed weight (g)	Bed temp. (K)	Gas flow into bed (mol/s)
208	N <sub>2</sub>	0.050–0.060	11.6	5.06	77	$3.0 \times 10^{-8}$
237	N <sub>2</sub>	0.060–0.080	9.5	4.12	77	$2.5 \times 10^{-8}$
238	N <sub>2</sub>	0.060–0.080	9.5	4.12	77	$1.2 \times 10^{-8}$
217	CO <sub>2</sub>	0.050–0.060	10.8	4.69	198	$3.3 \times 10^{-8}$
218	CO <sub>2</sub>	0.050–0.060	10.8	4.69	198	$3.9 \times 10^{-8}$
225	CO <sub>2</sub>	0.060–0.080	10.0	4.33	198	$3.9 \times 10^{-8}$
227	CO <sub>2</sub>	0.060–0.080	10.0	4.33	198	$3.3 \times 10^{-8}$

**Table 2: Constants and parameters used in the proposed cryosorption pump model**

Description	Symbol	Value	Reference
Bed cross-sectional area	$A$	0.472 cm <sup>2</sup>	Crabb, Perona, 1985
Bed depth	$L$	see Table 1	Crabb, Perona, 1985
Bed temperature	$T_b$	see Table 1	Crabb, Perona, 1985
Sorbate feed rate	$Q$	see Table 1	Crabb, Perona, 1985
Ambient temperature	$T_a$	300 K	Crabb, Perona, 1985
Headspace volume	$V$	200 cm <sup>3</sup>	Crabb, Perona, 1985
Zeolite crystal density	$\rho_z$	2.0 g/cm <sup>3</sup>	Breck, 1974
Effective crystal radius	$R$	0.00012 cm	Crabb, Perona, 1985
Fraction of bed occupied by crystals	$\theta_z$	0.40	Breck, 1974
Fraction of bed available to gas	$\theta_G$	0.54	Breck, 1974
Bulk density of mol. sieve	$\rho_b$	0.92 g/cm <sup>3</sup>	Crabb, Perona, 1985
Mean pore radius	$r_p$	0.0032 cm	Crabb, Perona, 1985

*Parameters that Depend on the Sorbate Gas*

		CO <sub>2</sub>	N <sub>2</sub>	
Molecular weight of gas	$M$	44.0	28.0 g/mol	
Langmuir equilibrium constant	$k$	4.0	1.0 torr	Crabb, Perona, 1985
Langmuir saturation constant	$q_m$	0.004	0.0003 mol/g	Crabb, Perona, 1985
Lennard-Jones collision diameter	$\sigma$	3.941	$3.798 \times 10^{-10}$ m	Sherwood et al. 1975
Lennard-Jones collision potential	$\Omega$	1.43	1.39	Sherwood et al. 1975
Limiting zeolitic diffusivity	$D_0$	$10^{-13}$	cm <sup>2</sup> /s	Yucel and Ruthven, 1980
	$D_0$		$< 10^{-20}$ cm <sup>2</sup> /s	Crabb, Perona, 1985

his text (1974). The bulk density of the bed is computed from the bed height and bed weight measurements given by Crabb and Perona (1985). Langmuir isotherm constants were obtained from Appendix C of Crabb and Perona's paper. As they point out, isotherm data for CO<sub>2</sub> and N<sub>2</sub> are rarely available for the conditions of temperature and pressure typical in cryosorption systems. Isotherm constants for both gases are extrapolated from pressures greater than 1 torr. Data for CO<sub>2</sub> was obtained by Crabb and Perona from the molecular sieve manufacturer, the W. R. Grace Co.; N<sub>2</sub> data were obtained from experiments they performed. Lennard-Jones constants for CO<sub>2</sub> and N<sub>2</sub> were obtained from the text by Sherwood, Pigford, and Wilke (1975). Values for the corrected zeolitic diffusivities of CO<sub>2</sub> and N<sub>2</sub> at cryosorption conditions were also difficult to obtain. Yucel and Ruthven (1980) and Ruthven in his book (1984) address the dependence of the limiting diffusivity on temperature for both CO<sub>2</sub> and N<sub>2</sub>. Cryogenic temperatures are outside the range of their experiments, but extrapolations can be made to obtain estimates.

When the model parameters from Table 2 are used, the model and the data collected by Crabb and Perona (1985) do not agree well. Fig. 9 shows the experimental results from Crabb and Perona (Run 218) and theoretical results based on the parameters in Table 2. The curves are typical of theoretical results for CO<sub>2</sub> using parameters obtained from the literature in that the predicted pressure rise is steeper than the experimental pressure rise, the estimated pressure drop is generally higher than that actually observed, and the ultimate predicted decrease in the pressure drop is more pronounced than the observed decrease. A solution for N<sub>2</sub>, using reported zeolitic diffusivities of  $< 10^{-20}$  cm<sup>2</sup>/s, could not be obtained; however, a solution using a larger value,  $10^{-12}$  cm<sup>2</sup>/s, is shown in Fig. 10.

A general physical interpretation of the disparity between the observed behavior and the model results is that the molecular sieve has a greater capacity for the sorbate gas than is predicted by the model. In the case of CO<sub>2</sub>, although the predicted results appear to have the correct general shape, a lack

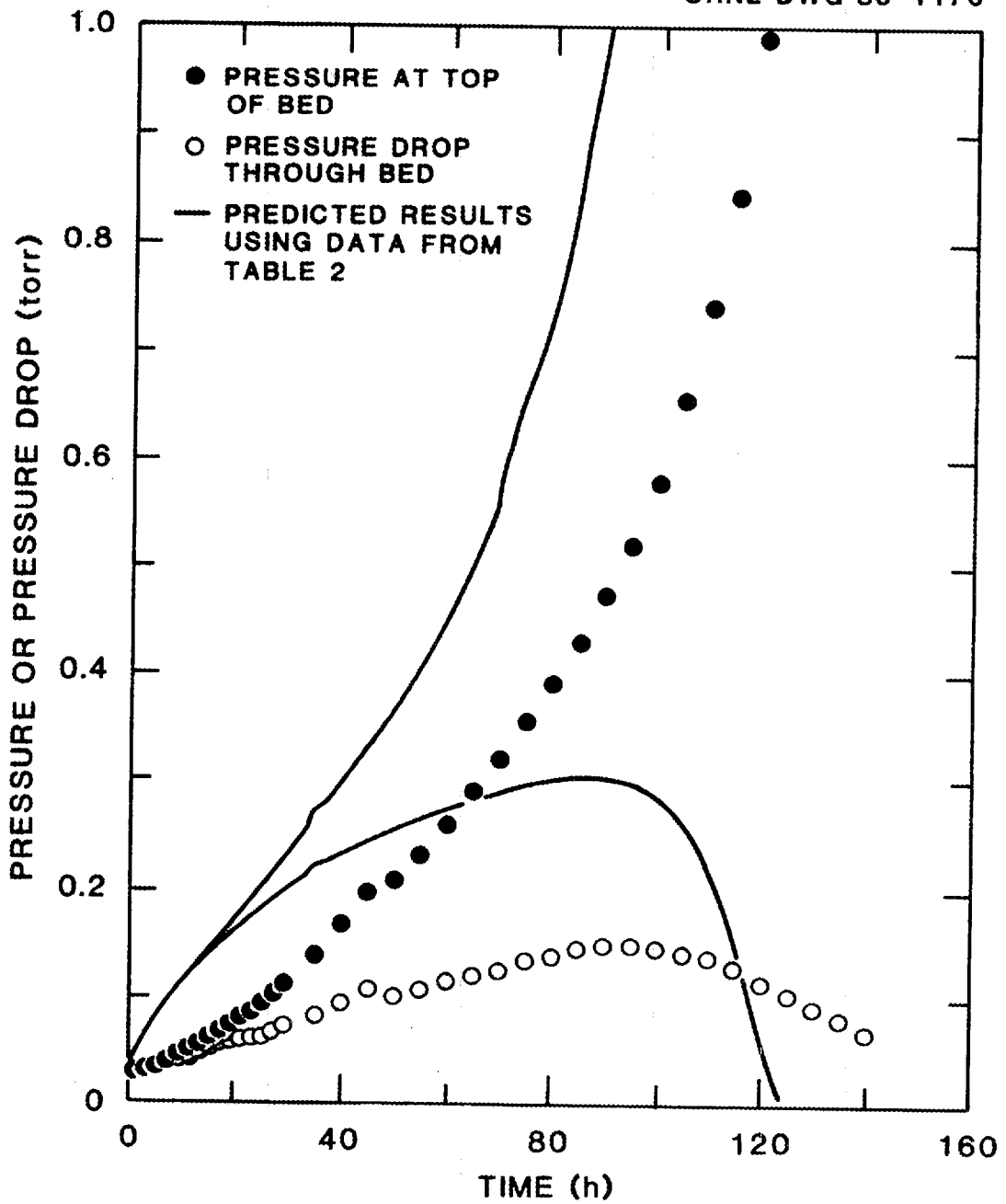


Fig. 9. Comparison of computed and observed results for  $\text{CO}_2$  [experimental data from Crabb and Perona run 218; computed results from proposed model using parameters from Table 2].

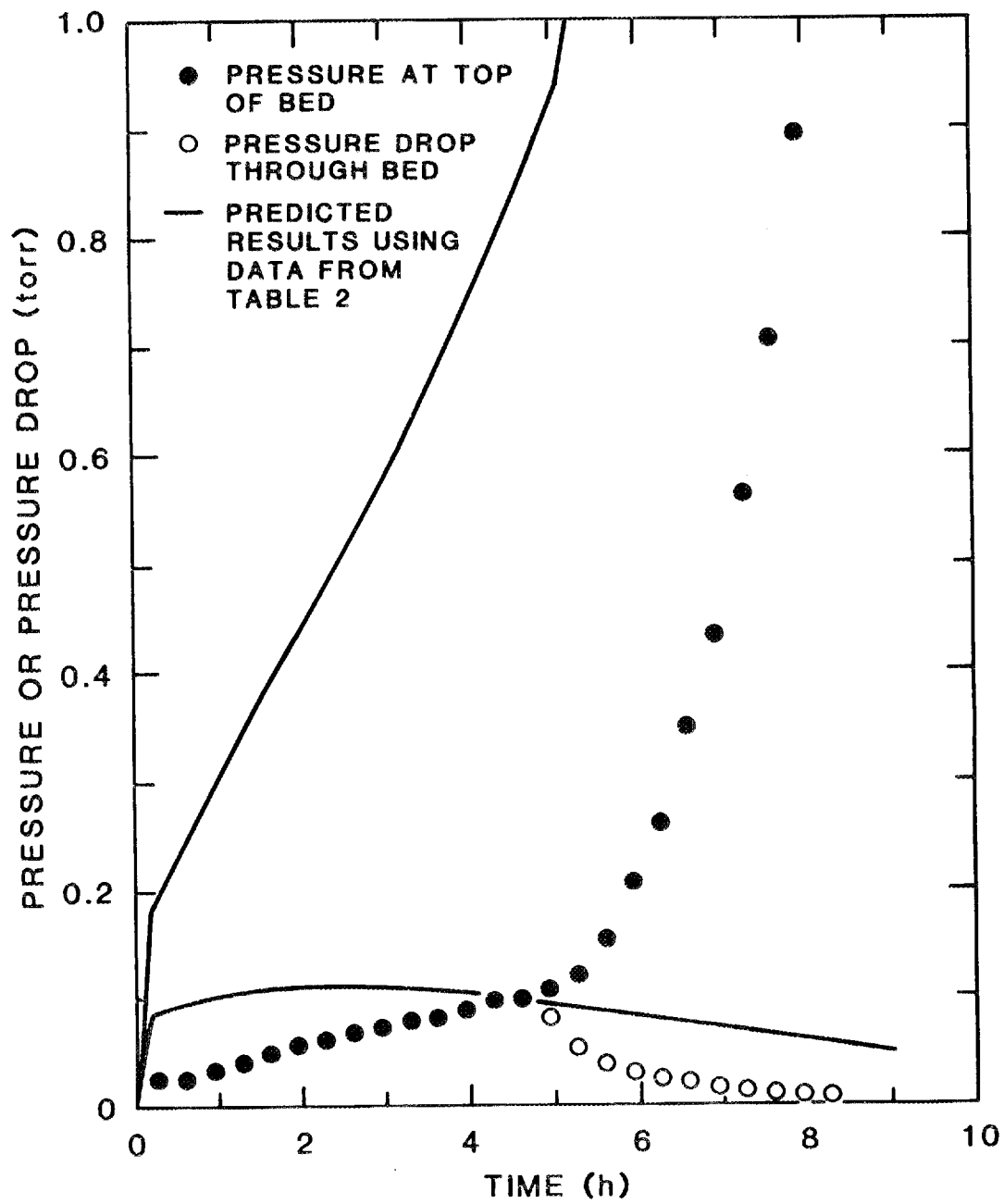


Fig. 10. Comparison of computed and observed results for  $N_2$  [experimental data from Crabb and Perona run 208; computed results from proposed model using parameters from Table 2].

of sorption capacity is suggested by the short duration and sharp breakthrough predicted by the model. The  $N_2$  results are also similar to the experimental data in feature, although they obviously do not provide a close match with the curves. Nitrogen's predicted sorption characteristics can be characterized by an initial linear increase in pressure, followed by an approach to saturation that is distinctly different from experimental observations. The initial decrease in the slope of the pressure curves appears to correspond to the pressure rise and its effect on the pore diffusion coefficient. The ultimate pressure rise corresponds to saturation of the sorbent and breakthrough of the sorbate to the bottom of the bed. A well-defined breakthrough point, identifiable by a sharp decrease in the pressure drop through the bed and evident on Fig. 9, is consistent with underestimation of the sorbent uptake capacity. A well-defined breakthrough is not evident in Fig. 10, because saturation is not predicted in the time period shown.

Given the extrapolated isotherm data and diffusivities, and using model parameters collected from the four sources listed in Table 2, a good match between the predicted and observed results would have been a fortuitous occurrence. Of the model parameters listed in Table 2, the Langmuir constants, mean pore radius, and zeolitic diffusivity are subject to the most uncertainty for the reasons already discussed.

Disparities between predicted and observed results were resolved, to as great a degree as possible, by manipulating these parameters. In general, the approach taken here is similar to that taken by Crabb et al. (1986). Parameters adjusted to improve the agreement between the model proposed here and the Crabb and Perona data appear to be somewhat closer to values suggested in the literature, particularly in the case of the zeolitic diffusivities, than those obtained by Crabb et al. Both the original and the adjusted parameters are shown in Table 3.

Predicted and observed results for  $CO_2$  runs 217, 218, 225, and 227, using adjusted values for  $k$ ,  $q_m$ ,  $r_p$ , and  $D_0$ , are shown in Figs. 11 through 14, respectively. The improved match between experimental and computed results is the

**Table 3: Initial and adjusted model parameters**

Parameter	Initial value	Adjusted value
<i>CO<sub>2</sub> Runs</i>		
$k$	4.0 torr <sup>-1</sup>	4.0 torr <sup>-1</sup>
$q_m$	0.0040 mol/g	0.0048 mol/g
$r_p$	0.0032 cm	0.0064 cm
$D_0$	$1 \times 10^{-13}$ cm <sup>2</sup> /s	$1 \times 10^{-13}$ cm <sup>2</sup> /s
<i>N<sub>2</sub> Runs</i>		
$k$	1.0 torr <sup>-1</sup>	20.0 torr <sup>-1</sup>
$q_m$	0.0003 mol/g	0.00019 mol/g
$r_p$	0.0032 cm	0.0064 cm
$D_0$	$1 \times 10^{-13}$ cm <sup>2</sup> /s	$1 \times 10^{-11}$ cm <sup>2</sup> /s

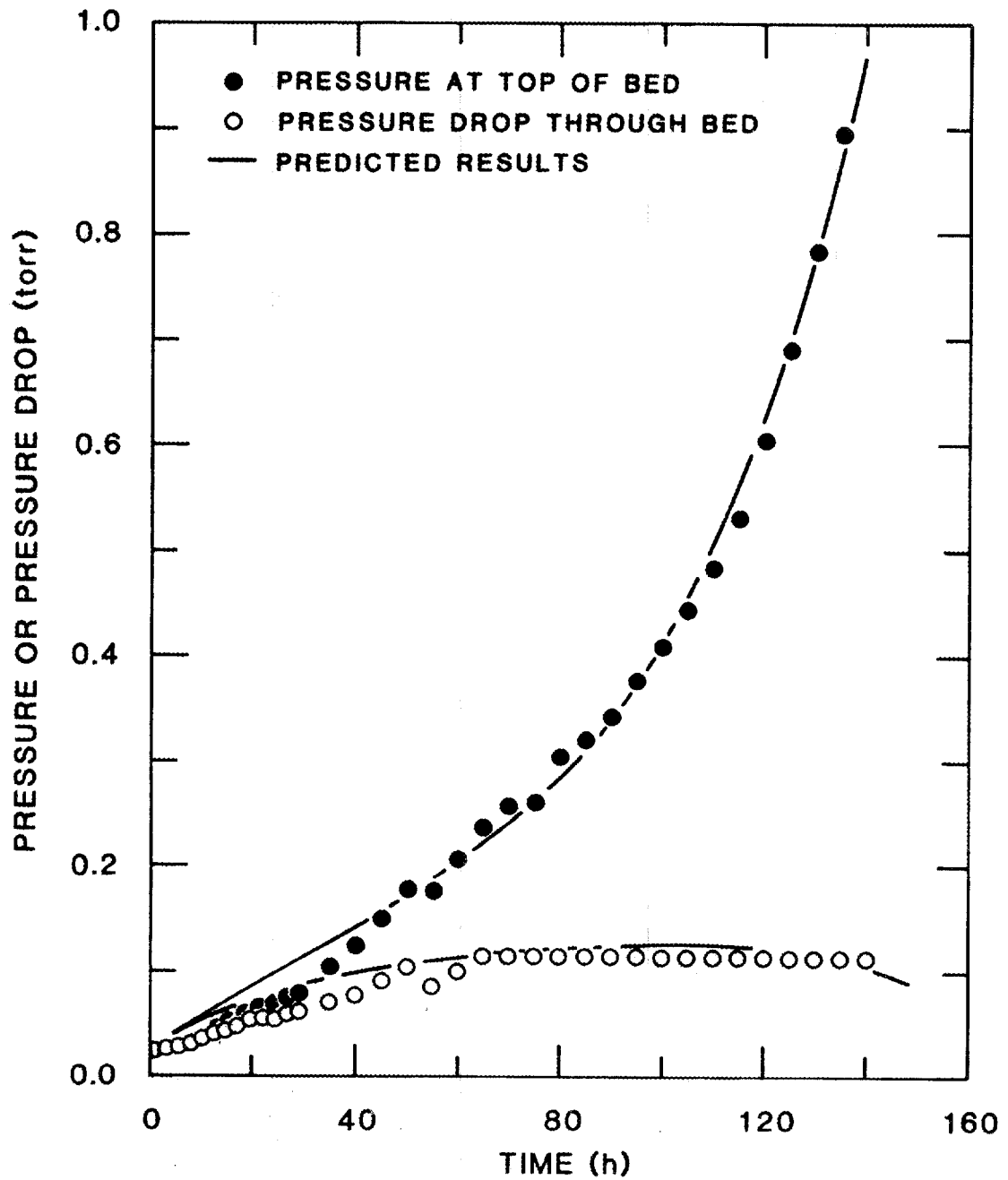


Fig. 11. Comparison of computed and observed results for CO<sub>2</sub> [experimental data from Crabb and Perona (1985) Run 217; computed results from proposed model using adjusted parameters shown in Table 3].

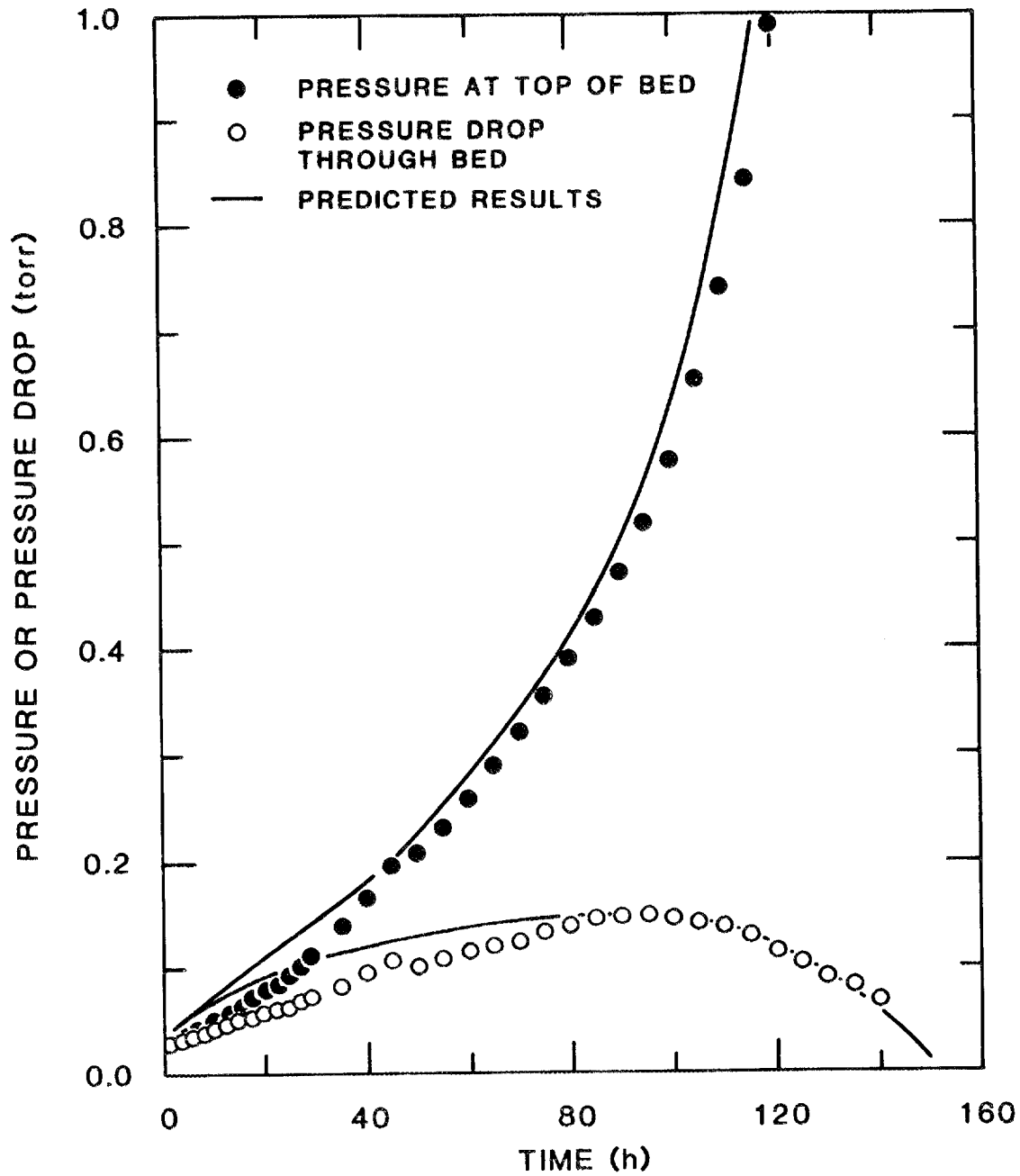


Fig. 12. Comparison of computed and observed results for CO<sub>2</sub> [experimental data from Crabb and Perona (1985) Run 218; computed results from proposed model using adjusted parameters shown in Table 3].

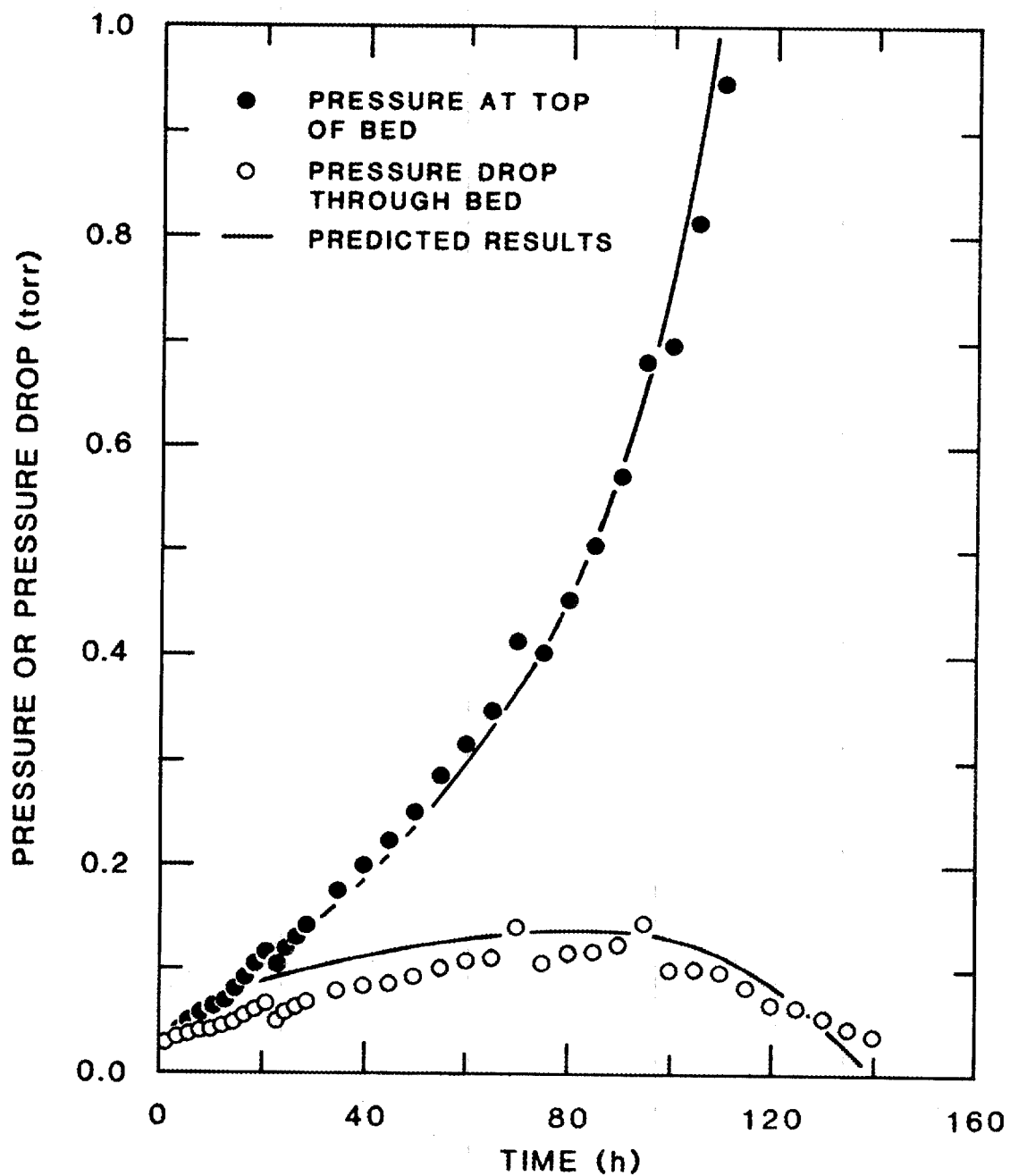


Fig. 13. Comparison of computed and observed results for  $\text{CO}_2$  [experimental data from Crabb and Perona (1985) Run 225; computed results from proposed model using adjusted parameters shown in Table 3].

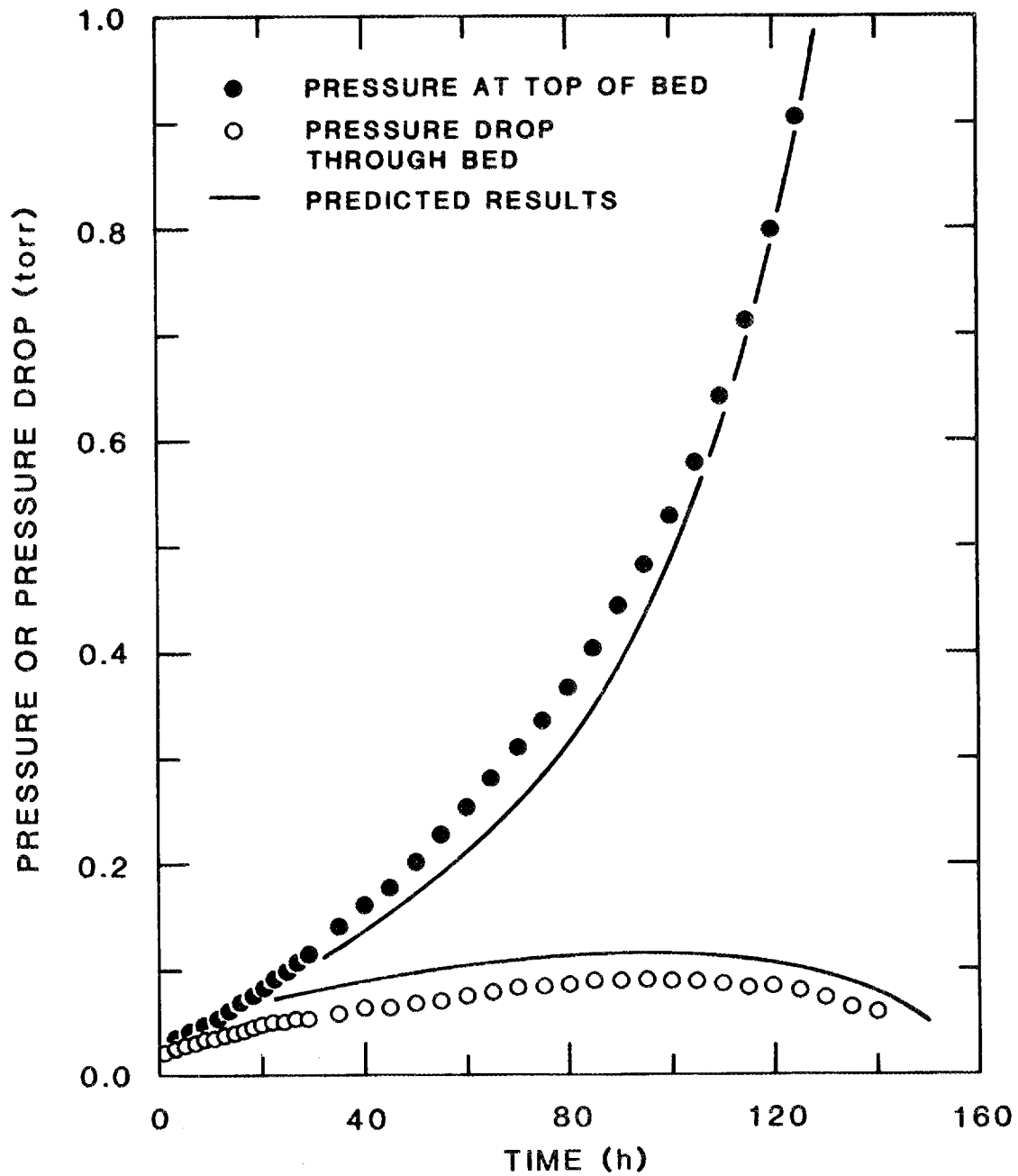


Fig. 14. Comparison of computed and observed results for  $\text{CO}_2$  [experimental data from Crabb and Perona (1985) Run 227; computed results from proposed model using adjusted parameters shown in Table 3].

result of a 20% increase in the Langmuir saturation constant,  $q_m$ , and a 100% increase in the pore diffusivity, from the parameter values given in Table 2. In physical terms, increases in  $q_m$  effectively increase the saturation capacity of the sorbent. Increasing values for  $r_p$  represent higher flow conductance through the bed, lower absolute values for the pressure drop, and shorter pressure-drop curves. The interdependence of the parameters  $q_m$  and  $r_p$  is discussed in Sect. A.3. Values for the Langmuir equilibrium constant,  $k$ , and the limiting diffusivity,  $D_0$ , were not changed from the values given in Table 2 for  $\text{CO}_2$ .

A good general agreement is seen between experimental and observed results for  $\text{CO}_2$ . Pressure and pressure-drop estimates for the first 20 of all runs are somewhat inflated, and the disparity appears to be greater for runs 217 and 218 than for runs 225 and 227. These two sets of runs are distinguished by differences in the molecular sieve particle diameter, bed height, and bed weight (see Table 1). The cause for this rather consistent bias is not clear, although it is unlikely to be the particle diameter. Runs 217 and 218, with smaller particles, could be assigned a commensurately smaller value for the mean pore radius. However, a smaller value for  $r_p$  would lessen the agreement with the observed results.

Figs. 15, 16, and 17 represent  $\text{N}_2$  runs 208, 237, and 238, respectively. Three observations based on these figures are made here. First, manipulation of three of the four "free parameters",  $k$ ,  $q_m$ , and  $r_p$ , significantly improved agreement between predicted and observed bed behavior. Second, more adjustment was required to obtain good agreement for the  $\text{N}_2$  data than for the  $\text{CO}_2$  data. And third, the characteristics of the  $\text{N}_2$  data are not completely described by the adjusted model. Other than the fact that solutions could not be obtained for values of  $D_0$  less than  $\sim 1 \times 10^{-11}$   $\text{cm}^2/\text{s}$ , predicted pressures in the bed were insensitive to changes in the limiting diffusivity over the range of values from  $1 \times 10^{-8}$  to  $1 \times 10^{-11}$   $\text{cm}^2/\text{s}$ . The observed  $\text{N}_2$  results were difficult to model because of sharp changes in the pressure and pressure drop as the bed approached saturation. To arrive at the predicted results shown in Figs. 15, 16, and 17, the value of  $k$  was 20 times greater,  $q_m$  was decreased by 37%, and  $r_p$

ORNL DWG 86-1182

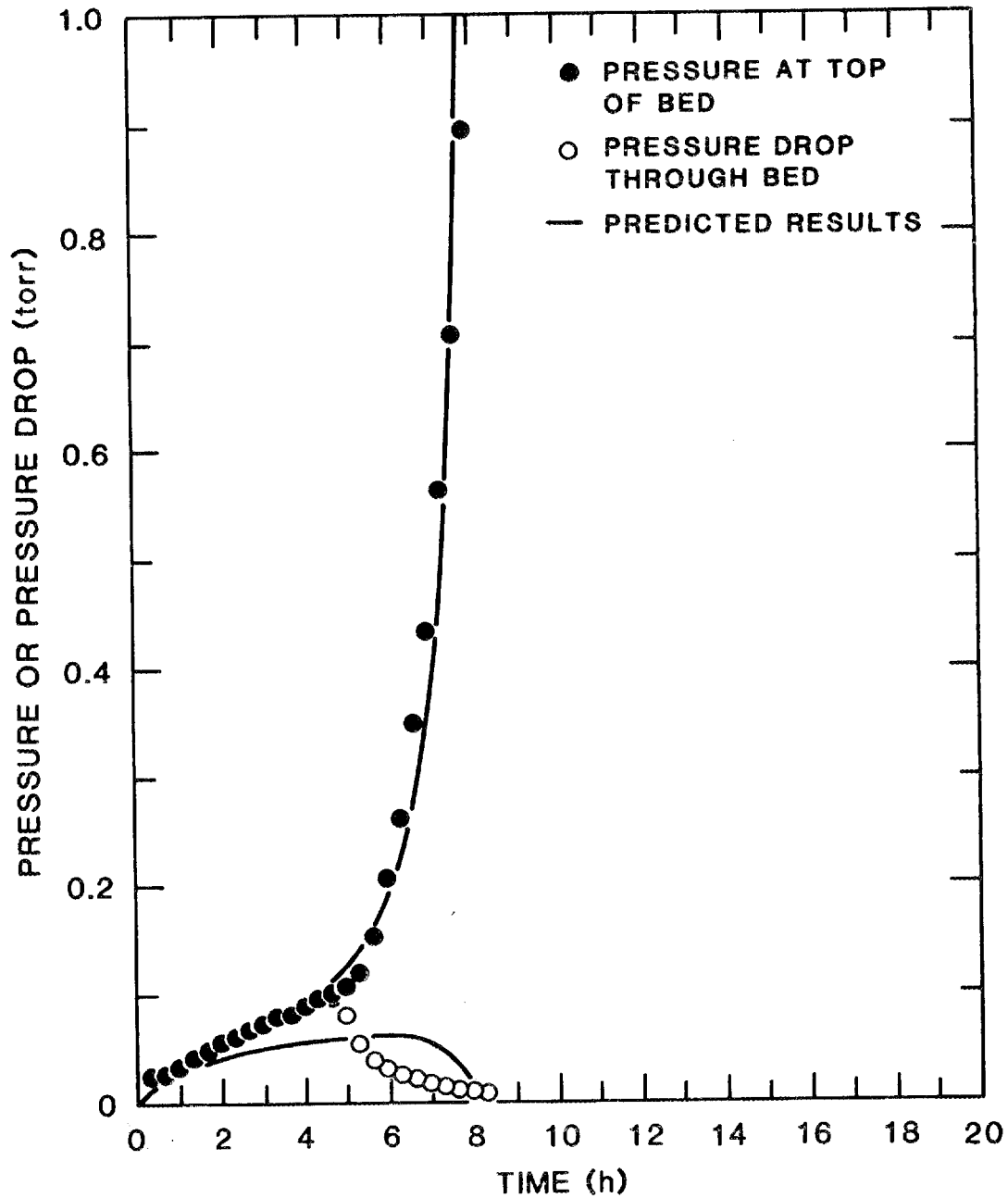


Fig. 15. Comparison of computed and observed results for  $N_2$  [experimental data from Crabb and Perona (1985) Run 208; computed results from proposed model using adjusted parameters shown in Table 3].

ORNL DWG 86-1183

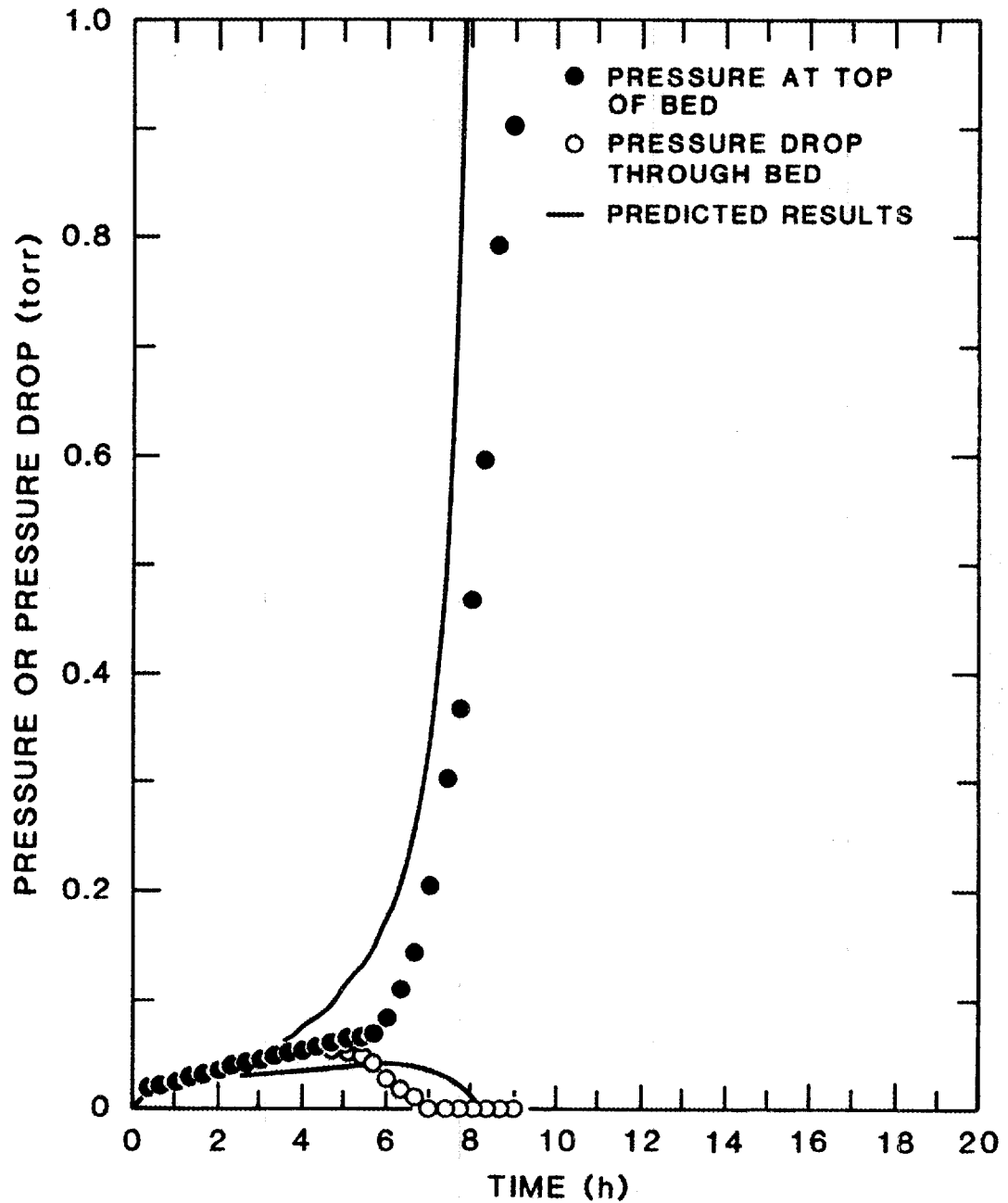


Fig. 16. Comparison of computed and observed results for  $N_2$  [experimental data from Crabb and Perona (1985) Run 237; computed results from proposed model using adjusted parameters shown in Table 3].

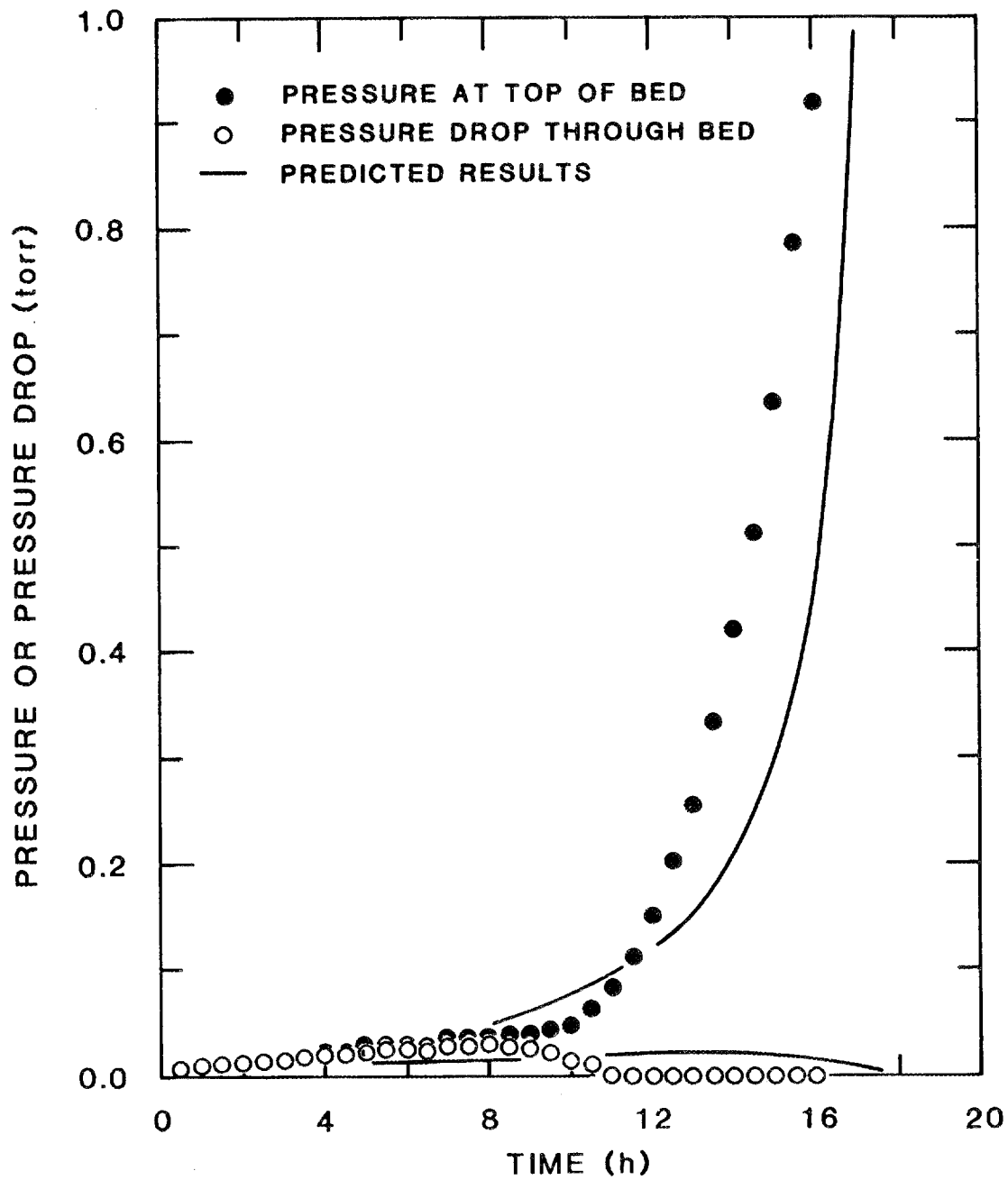


Fig. 17. Comparison of computed and observed results for  $N_2$  [experimental data from Crabb and Perona (1985) Run 238; computed results from proposed model using adjusted parameters shown in Table 3].

was increased by 100%.

The extremely low sorption capacity of zeolite 4A for  $N_2$  is well-documented. An extrapolation of data given by Ruthven (1984) to temperatures typical in this study implies that the limiting diffusivity is  $< 1 \times 10^{-20}$  cm<sup>2</sup>/s. Such a small value indicates that the sorption kinetics are relatively slow compared to the bed dynamics and that the system might be sufficiently modeled by assuming that the solids-loading profile in the crystals is independent of time. The adjustments to the Langmuir constants for  $N_2$  and the use of a large diffusivity, which was necessary to obtain a numerical solution, result in a sorbate concentration profile for  $N_2$  such as that illustrated by the solid curves in Fig. 18. The figure contrasts computed concentration profiles in a sorbent particle for  $CO_2$  and  $N_2$  at dimensionless times up to 0.5. Dimensionless time,  $\hat{t}$  is the ratio of chronological time to the time at which the pressure at the top of the bed reaches 1 torr. The relatively straight profiles for  $N_2$  suggest that the solids-loading for a sphere might be modeled simply as a function of pressure, which is the approach used by Crabb et al. (1986).

#### 4.3 SENSITIVITY OF $CO_2$ RESULTS TO MODEL PARAMETERS

Crabb et al. (1986) have discussed the sensitivity of their calculated results to changes in model parameters for the cryosorption of  $N_2$ . They found that the calculated effects of changes in the gas feed rate and bed length on pressure and pressure drop in the bed were consistent with the effects observed in experiments. They also examined the effects of four adjustable parameters, the fluid-phase diffusion coefficient, the solid-phase diffusivity, and the Langmuir constants on  $N_2$  sorption behavior. Experiments they performed using  $CO_2$  form the basis for the following discussion on the predicted and observed sensitivity of  $CO_2$  sorption behavior to changes in bed conditions and to changes in model parameters. In order to facilitate a quantitative discussion of the bed behavior, the pressure and pressure drop curves used thus far will be represented by two parameters: (1) the time required for the gas pressure at the top of the bed to reach 1 torr,

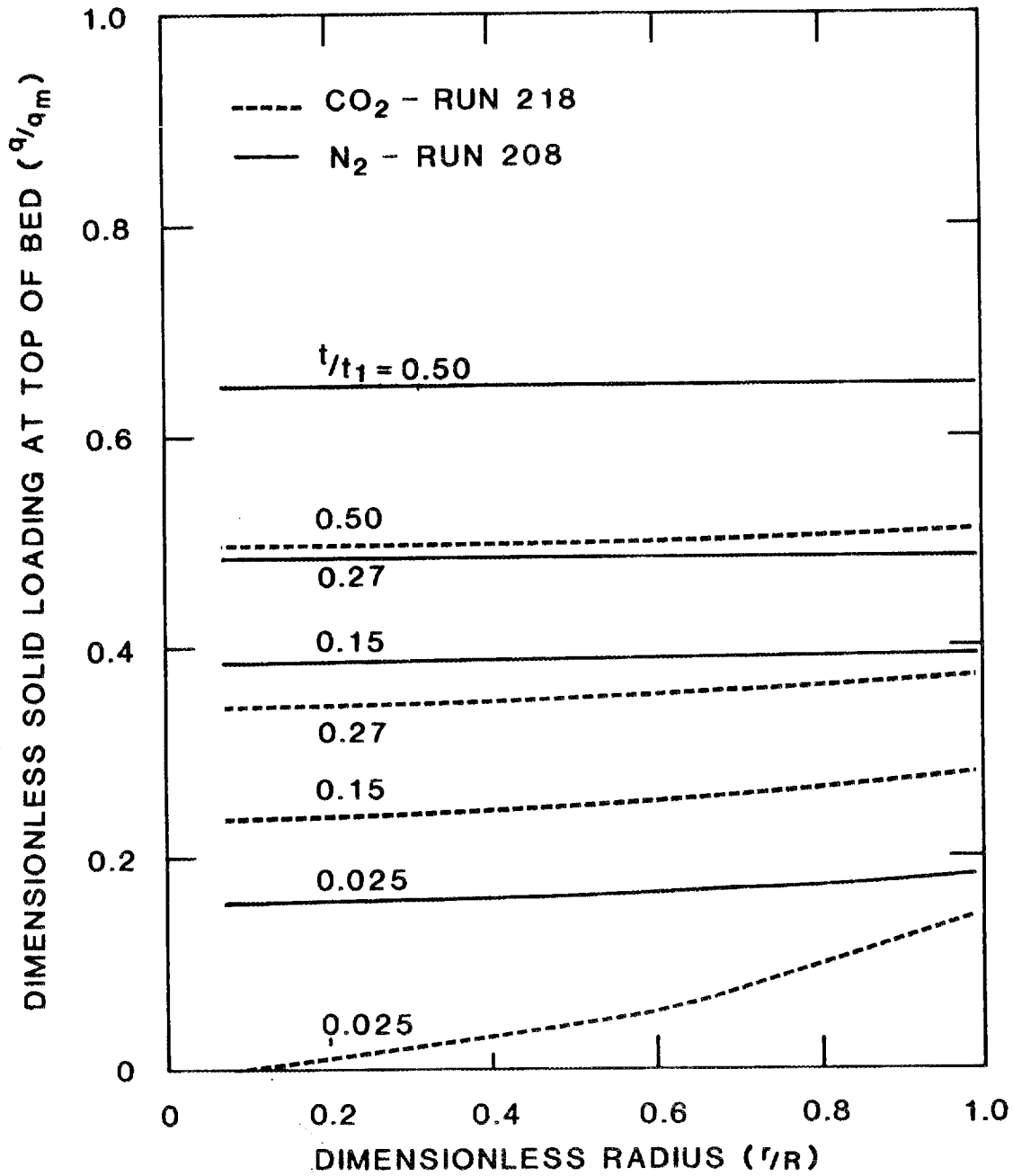


Fig. 18. Computed sorbate concentration profile in the solid for dimensionless times up to 0.5. Based on Runs 208 and 218 using parameters from Table 3.

henceforth referred to as the run time; and, (2) the maximum pressure drop, or  $\Delta p_{\max}$ . Mathematical "effects" are computed from experimental results in which one or more independent variables are systematically varied to produce a change in a dependent variable. In the following discussion, they are used to represent the sensitivity of the run time and  $\Delta p_{\max}$  (dependent variables) to changes in the bed configuration and the adjustable parameters (independent variables).

Differences among experimental results from runs 217, 218, 225, and 227 (Table 1) represent the effects of gas flow rate and bed height/particle diameter on sorption behavior. Table 4 summarizes the experimental and computed results in terms of the run time and  $\Delta p_{\max}$ . Based on the experimental results, the effect of the flow rate increase is a 19-h decrease in the run time, and the effect of increasing the bed depth/particle size is a 9-h increase in run time. The computed results indicate a 24-h decrease and an 8.5-h increase, respectively, for the same set of changes in conditions. The projected effect on the maximum pressure drop, as estimated from the experimental data, is an increase of 0.044 torr due to the flow increase and an increase of 0.014 torr due to the bed height/particle size increase. Comparable computed increases in  $\Delta p_{\max}$  from the model are 0.046 torr and 0.024 torr, respectively. These comparisons indicate that the model is in good agreement with the observed results. As expected, it predicts that increasing the throughput or decreasing the amount of sorbent in the bed shortens the bed life and that increasing the throughput and/or the amount of sorbent increases the  $\Delta p_{\max}$  in the bed.

A similar analysis can be done to estimate the computed effects of other model parameters on the behavior of the bed. Table 5 summarizes the results of calculations performed to quantify the effects of three adjustable parameters,  $k$ ,  $q_m$ , and  $r_p$ , on the run time and on the  $\Delta p_{\max}$  for the CO<sub>2</sub> runs. Computer calculations were made for all maximum and minimum parameter values in the ranges given in Table 5. Using relatively simple analysis of variance techniques, the results can be expressed in terms of the effects of  $k$ ,  $q_m$ , and  $r_p$  and their

**Table 4. Observed and predicted run time and  $\Delta p_{\max}$  as a function of feed rate and bed height/particle diameter**

Run No.	Flow rate (mol/s)	Bed height/particle size (cm/mm)	Observed		Predicted	
			$t_1^a$ (h)	$\Delta p_{\max}^b$ (torr)	$t_1$ (h)	$\Delta p_{\max}$ (torr)
217	$3.3 \times 10^{-8}$	10.0/0.50-0.60	140	0.116 <sup>c</sup>	140	0.124
218	$3.9 \times 10^{-8}$	10.0/0.50-0.60	120	0.149	115	0.148
227	$3.3 \times 10^{-8}$	10.8/0.60-0.80	130	0.091	130	0.113
225	$3.9 \times 10^{-8}$	10.8/0.60-0.80	112	0.145	108	0.135

<sup>a</sup> $t_1$  = time required for the pressure at the top of the bed to reach 1 torr.

<sup>b</sup> $\Delta p_{\max}$  = maximum pressure drop.

<sup>c</sup> Based on the appearance of the data, this result is questionable, and may be conservative.

Table 5. Computed effects of  $k$ ,  $q_m$ , and  $r_p$  on run time and  $\Delta p_{\max}$ 

Parameter <sup>a</sup>	Change in $t_1$ required to reach 1 torr <sup>b</sup> (h)	Change in $\Delta p_{\max}$ <sup>c</sup> (torr)
$k$	26.5	0.007
$q_m$	36.1	0.000
$r_p$	12.4	-0.204
$k \times q_m$	5.1	0.000

<sup>a</sup> Maximum and minimum values from which the above effects were calculated are:

$$k : 4.0 \pm 2.0 \text{ torr}^{-1}$$

$$q_m : 0.0048 \pm 0.0008 \text{ mol/g}$$

$$r_p : 0.0064 \pm 0.0032 \text{ cm.}$$

<sup>b</sup> $t_1$  = time required for pressure at the top of the bed to reach 1 torr.

<sup>c</sup> $\Delta p_{\max}$  = maximum pressure drop through bed.

interactions on the run time and  $\Delta p_{\max}$ . Consideration of the interactions is useful to indicate whether parameters act independently or exhibit synergism. The estimated effects apply only to the parameter ranges shown in Table 5, and only linear effects have been computed.

The effects shown in the table indicate that increasing the Langmuir constants causes a strong corresponding increase in the run time. As expected, the saturation constant,  $q_m$ , produces the most pronounced effect because it is the parameter most closely related to the capacity of the sorbent.

Increasing the mean pore radius also increases the run time, though to a lesser degree. In addition, there is a small interaction between  $k$  and  $q_m$ , which indicates that the combined increase caused by  $k$  and  $q_m$  is greater than the sum of their individual effects. The calculations for Table 5 also show that only one of the three parameters considered,  $r_p$ , has a significant effect on  $\Delta p_{\max}$ .

## 5. CONCLUSIONS AND RECOMMENDATIONS

Orthogonal collocation, in conjunction with the ordinary differential equation solver LSODE, is an effective method for solving the parabolic partial differential equations that describe unsteady-state cryosorption in a fixed bed of zeolite molecular sieves. Solutions were obtained using the model of Crabb and Perona (1985) and using a proposed model with more detailed treatment of the solids diffusion equation. Computing times and run costs were  $\sim 50$  times less than those reported by Crabb and Perona, for the use of finite differences. Simulations of  $N_2$  adsorption using diffusivities of  $10^{-12} \text{ cm}^2/\text{s}$  could not be completed. A possible cause is that the rate of change of the solids loading decreased to be approximately equal to the errors incurred in calculating the derivatives or the Jacobian matrix. A more rigorous numerical implementation of the model, including the expression of the model equations in matrix form and a direct calculation of the Jacobian matrix, would facilitate a more complete numerical analysis of the equations.

After some manipulation of the equilibrium adsorption isotherm constants and the mean pore radius, which is directly related to the gas-phase diffusion coefficient, good agreement was obtained between the proposed model and the  $CO_2$  sorption data taken by Crabb and Perona (1985). Our calculated results did not agree as well with the  $N_2$  data, and we were unable to make calculations using the literature values for zeolitic diffusivity of  $N_2$ . Compensatory adjustments to other parameters yielded a reasonable overall fit, but the sharp changes in pressure and pressure drop exhibited by  $N_2$  data were not matched in the calculated results.

An assumption throughout the development of this analysis has been that the micropore diffusional resistance within the zeolite crystals is controlling in the cases of  $CO_2$  and  $N_2$ , and that equilibrium with the bulk phase at the crystal surface is instantaneous. The results presented here support such an assumption for  $CO_2$ . However, because  $N_2$  is adsorbed at lower rates and in

such small quantities in zeolite 4A, it appears that the macropore diffusivity may be controlling for  $N_2$ . Crabb and Perona (1985) used such a basis for their calculations and obtained a reasonably good fit with their  $N_2$  data.

Additional work in this area would certainly be enhanced by the computer implementation of a model capable of representing diffusional resistances in the intercrystalline voids as well as within the crystals. Computation of the instantaneous mean accumulation in a crystal by using the flux at the crystal surface is an efficient procedure. However, it may contribute to the failure of reaching a solution for low  $N_2$  diffusivity values, while an integration approach for calculating  $\partial\bar{q}/\partial t$  might succeed. If an efficient means of implementing the integral approach in coordination with Gear's method can be developed, the utility of the computer model might be expanded.

Verification of these results, and application of this modeling technique to the cryosorption of other gases, could be enhanced by the availability of equilibrium adsorption isotherm data at cryogenic conditions. Such data would reduce the uncertainty associated with the equilibrium constants and focus attention on the roles of diffusional resistances and on differences in sorbate behavior. Further adaptations to this model could facilitate comparisons with data from a wide range of adsorption applications. In his text, Ruthven (1984) presents data from a number of experiments at elevated pressures and temperatures that could provide a source of verification for a modified adsorption model.

## REFERENCES

- Barrer, R. M. 1978. *Zeolites and Clay Minerals as Sorbents and Molecular Sieves*, Academic Press, London.
- Bird, R. B., Stewart, W. E., and Lightfoot, E. N. 1960. *Transport Phenomena*, Wiley, New York.
- Breck, D. W. 1974. *Zeolite Molecular Sieves*, Wiley, New York.
- Carnahan, B., Luther, H. A., and Wilkes, J. O., 1969. *Applied Numerical Methods*, Wiley, New York.
- Crabb, K. S., and Perona, J. J. 1985. "Mass Transfer in Vacuum Sorption Pumping of Pure Gases on Molecular Sieves," Oak Ridge National Laboratory, Oak Ridge, Tenn., ORNL-6092.
- Crabb, K. S., Perona, J. J., Byers, C. H., and Watson, J. S. 1986. "Vacuum Sorption Pumping Studies with Pure Gases on Molecular Sieves", *AIChE J.*, **32**, 255.
- Dennison, R. W., and Gray, G. R. 1979. "Cryogenic Versus Turbomolecular Pumping in a Sputtering Application," *J. Vac. Sci. Technol.*, **16**(2).
- Ferguson, N. B., and Finlayson, B. A. 1970. "Transient Chemical Reaction Analysis by Orthogonal Collocation," *Chem. Eng. J.*, **1**, 327.
- Finlayson, B. A. 1971. "Packed Bed Reactor Analysis by Orthogonal Collocation," *Chem. Eng. Sci.*, **26**, 1081.
- Finlayson, B. A. 1972. *The Method of Weighted Residuals and Variational Principles*, McGraw-Hill Book Co., New York.
- Finlayson, B. A. 1980. *Nonlinear Analysis in Chemical Engineering*, McGraw-Hill Book Co., New York.
- Fisher, P. W., and Watson, J. S. 1976. "Cryosorption Vacuum Pumping of Deuterium, Helium, and Hydrogen at 4.2 K for Controlled Thermonuclear Reaction Applications," Proceedings of the 24th Conference on Remote Systems Technology.
- Forsythe, G. E., Malcolm, M. A., and Moller, C. B. 1977. *Computer Methods for Mathematical Computations*, Prentice-Hall, New Jersey.
- Garg, D. R., and Ruthven, D. M. 1973a. "Theoretical Prediction of Break-through Curves for Molecular Sieve Adsorption Columns - I: Asymptotic Solutions," *Chem. Eng. Sci.*, **28**, 791.
- Garg, D. R., and Ruthven, D. M. 1973b. "Theoretical Prediction of Break-through Curves for Molecular Sieve Adsorption Columns - II: General Isothermal

- Solution for Micropore Diffusion Control," *Chem. Eng. Sci.*, **28**, 799.
- Garg, D. R., and Ruthven, D. M. 1974. "The Performance of Molecular Sieve Adsorption Columns: Systems with Micropore Diffusion Control," *Chem. Eng. Sci.*, **29**, 571.
- Holland, C. D., and Liapis, A. I. 1983. *Computer Methods for Solving Dynamic Separation Problems*, McGraw-Hill, New York.
- Hseuh, H. C., and Worwetz, H. A. 1981. "Performance of BNL-TSTA Compound Cryopump," *J. Vac. Sci. Technol.*, **18**, 1131.
- Lapidus, L. 1962. *Digital Computation for Chemical Engineers*, McGraw-Hill, New York.
- McBain, J. W. 1932. *The Sorption of Gases and Vapors by Solids*, Rutledge and Sons, London.
- Michelsen, M. L., and Villadsen, J. 1972. "A Convenient Computational Procedure for Collocation Constants," *Chem. Eng. J.*, **4**, 64.
- Michelsen, M. L., and Villadsen, J. 1978. *Solution of Differential Equation Models by Polynomial Approximation*, Prentice-Hall, New Jersey.
- Raghavan, N. S., and Ruthven, D. M. 1983. "Numerical Simulation of a Fixed-Bed Adsorption Column by the Method of Orthogonal Collocation," *AIChE J.*, **29**, 922.
- Reed, T. B., and Breck, D. W. 1956. "Crystalline Zeolites. II. Crystalline Structure of Synthetic Zeolite, Type A", *J. Amer. Chem. Soc.*, **78**, 5972.
- Ruthven, D. M. 1984. *Principles of Adsorption and Adsorption Processes*, Wiley, New York.
- Ruthven, D. M., and Loughlin, K. F. 1971a. "The Effect of Crystalline Shape and Size Distribution on Diffusion Measurements in Zeolite Molecular Sieves," *Chem. Eng. Sci.*, **26**, 577.
- Ruthven, D. M., and Loughlin, K. F. 1971b. "The Sorption and Diffusion of n-Butane in Linde 5A Molecular Sieve," *Chem. Eng. Sci.*, **26**, 1145.
- Sherwood, T. K., Pigford, R. L., and Wilke, C.R. 1975. *Mass Transfer*, McGraw-Hill, New York.
- Stern, S. A., and DiPaolo, F. S. 1969. "Cryosorption Pumping of Air on Molecular Sieves at 77 K - The Achievable Vacuum," *J. Vac. Sci. Technol.*, **6**, 941.
- Villadsen, J. V., and Stewart, W. E. 1967. "Solution of Boundary-Value Problems by Orthogonal Collocation," *Chem. Eng. Sci.*, **22**, 1483.

Visser, J., and Scheer, J. J. 1979. "Twenty Kelvin Cryopumping in Magnetron Sputtering Systems", *J. Vac. Sci. Technol.*, **16**, 734.

Visser, J., and Scheer, J. J. 1981. "A Cryosorption-Pumped Rapid Cycle UHV System," *J. Vac. Sci. Technol.*, **19**, 122.

Wheeler, W. 1974. "Abstract: Some Applications of Large Sorption Pumps," *J. Vac. Sci. Technol.*, **11**, 1.

Yucel, H., and Ruthven, D. M. 1980. "Diffusion of CO<sub>2</sub> in 4A and 5A Zeolite Crystals," *J. Coll. Int. Sci.*, **74**, 186.

**APPENDICES**

## APPENDIX A: DEVELOPMENT OF MODEL EQUATIONS USING ORTHOGONAL COLLOCATION

### A.1 TRIAL SOLUTION EQUATIONS

This appendix describes the transformation of the model equations and their boundary conditions into a set of discretized ordinary differential equations (ODEs). Much of the information presented here is collated from the text by Michelsen and Villadsen (1978) and the paper by Raghavan and Ruthven (1980).

The dimensionless polynomial trial functions,  $p(z)$  and  $q(r)$ , are written as

$$p_{N+2}(z, t) = (1 - z) p(0, t) + z p(1, t) + z p(1, t) + z(1 - z) \sum_{i=1}^N a_i(t) z^i, \quad (\text{A1})$$

for the pressure, and

$$q_{M+1}(z, r, t) = q(z, 1, t) + (1 - r) \sum_{i=1}^M b_i(t) r^i, \quad (\text{A2})$$

for the solids loading. The use of "hatted" notation, such as  $\hat{q}$ , that is used in the text to denote dimensionless variables is omitted here. The variables  $p$  and  $q$  are assumed to be dimensionless unless stated otherwise.

The zeros of the polynomials are collocation points at which the solutions are represented. The parameters,  $N$  and  $M$ , are the number of interior collocation points in the bed and in a crystal. Boundary conditions at the top and bottom of the bed, at  $z = 0$  and  $z = 1$ , are incorporated with the term  $z(1 - z)$ ; the condition at the crystal surface is included with the term  $(1 - r)$ . Henceforth,  $p(z, t)$  and  $q(z, r, t)$  will be written simply as  $p(z)$  and  $q(r)$ , and the dependence of the trial solution on time will be understood.

When differentiated and substituted into the model equations, the arbitrary polynomials  $p_{N+2}(z)$  and  $q_{M+1}(r)$  offer no particular advantage in terms of solution accuracy. Villadsen and Stewart (1967) showed that if collocation points are zeros of Jacobi polynomials, then the solution approximation is optimal in

the sense that the order of the approximation is maximized. Equations (A1) and (A2) can be written in terms of the Jacobi polynomials,  $J_N(x)$ , as follows,

$$p_{n+2}(z) = (1-z)p(0) + zp(1) + z(1-z) \sum_{i=1}^N c_i \cdot J_i(z), \quad (\text{A3})$$

$$q_{M+1}(r) = q(1) + (1-r) \sum_{i=1}^N d_i \cdot J_i(r), \quad (\text{A4})$$

where  $J_i(x)$  is an  $i^{\text{th}}$  degree polynomial of the form

$$J_i^{(\alpha, \beta)}(x) = \gamma_i x^i - \gamma_{i-1} x^{i-1} + \gamma_{i-2} x^{i-2} - \dots + (-1)^i, \quad (\text{A5})$$

that satisfies the orthogonality relation

$$\int_0^1 x^\beta (1-x)^\alpha J_i(x) J_j(x) dx = 0, \quad i \neq j. \quad (\text{A6})$$

Michelsen and Villadsen refer to Eqs. (A3) and (A4) above as node polynomials. The  $a_i$  and  $c_i$ ,  $b_i$  and  $d_i$  are related by the individual Jacobi polynomials. The  $\gamma_i$  may be calculated using Eq. (A6) with  $J_0(x) = 1$ , but simpler recursive formulas exist. However, the polynomial coefficients in Eqs. (A3) and (A4) are of less interest than the value of the polynomial and its derivative at specific values of  $z$  and  $r$ . The following recursive formula can be used to evaluate  $J_i(x_j)$  and  $J'_i(x_j)$ ,

$$J_i(x_j) = (g_i - x_j) J_{i-1}(x_j) - h_i J_{i-2}(x_j), \quad (\text{A7})$$

$$J'_i(x_j) = (g_i - x_j) J'_{i-1}(x_j) - h_i J'_{i-2}(x_j) - J_{i-1}(x_j), \quad (\text{A8})$$

where  $j = 1, 2, \dots, i$ ;  $J_{-1}(x) = 0$ ,  $J_0(x) = 1$ ,  $\alpha, \beta > -1$ ,

$$g_1 = \frac{\beta + 1}{\alpha + \beta + 2}.$$

For  $i > 1$ ,  $g_i = \frac{1}{2} \left[ 1 - \frac{\alpha^2 - \beta^2}{(2i + \alpha + \beta - 1)^2 - 1} \right].$

$$h_1 = 0, \quad h_2 = \frac{(\alpha + 1)(\beta + 1)}{(\alpha + \beta + 3)(\alpha + \beta + 2)^2},$$

and for  $i > 2$

$$h_i = \frac{(i-1)(i+\alpha-1)(i+\beta-1)(i+\alpha+\beta-1)}{(2i+\alpha+\beta-1)(2i+\alpha+\beta-2)^2(2i+\alpha+\beta-3)}.$$

The  $N$  and  $M$  interior collocation points defined by the zeros of Eqs. (A3) and (A4) are computed using Newton's method, the recursive relationships of Eqs. (A7) and (A8), and some useful properties of Jacobi polynomials. The zeros of the Jacobi polynomials in Eq. (A3),  $(z_2, z_3, \dots, z_{N+1})$ , and in Eq. (A4),  $(r_1, r_2, r_3, \dots, r_M)$ , are real, distinct, and lie in the interval  $(0, 1)$ . Further, a Newton iteration started from  $x = 0$  will converge to the smallest zero from below, because  $|J'_i(x)|$  is a monotonically decreasing function on  $(-\infty, x_1)$ , where  $x_1$  is the smallest root. When the first root is found, it can be extracted using

$$G_{i-1}(x) = \frac{J(x)}{(x-x_i)}, \quad (\text{A9})$$

to yield the polynomial  $G_{i-1}(x)$  of the next lower degree, which is also decreasing on  $(-\infty, x_2)$ . This root suppression process is repeated for each zero, with

$$G_{i-k}(x) = \frac{J_i(x)}{\prod_{k=1}^i (x-x_i)}, \quad (\text{A10})$$

until all the zeros are determined. Michelsen and Villadsen give the following Newton iteration scheme for computing the  $(i+1)$  iterate of the  $(k+1)$  zero:

$$x_{k+1}^{(i+1)} = x_k^{(i)} + \frac{\frac{J_N(x)}{J'_N(x)}}{1 - \frac{J_N(x)}{J'_N(x)} \sum_{j=1}^k \frac{1}{(x-x_j)}}. \quad (\text{A11})$$

## A.2 APPLICATION OF THE TRIAL SOLUTIONS TO THE MODEL EQUATIONS

Finding the zeros of the node polynomials is necessary so the derivatives of the node polynomial at the collocation points can be expressed in terms of the solution at the collocation points. If  $\partial p/\partial z$  and  $\partial^2 p/\partial z^2$  are expressed in terms of  $p$ , and  $\partial q/\partial r$  and  $\partial^2 q/\partial r^2$  are expressed in terms of  $q$ , then the model equations can be expressed and solved as an initial value problem with a set of ODEs in  $p$  and  $q$ .

The trial solutions defined by the  $N + 2$  and  $M + 1$  collocation points can be approximated using LaGrange interpolating polynomials,

$$p_{N+2}(z) = \sum_{i=1}^{N+2} l_i(z) \cdot p(z_i), \quad (\text{A12})$$

and

$$q_{M+1}(r) = \sum_{i=1}^{M+1} l_i(r) \cdot q(r_i), \quad (\text{A13})$$

where

$$l_i(z) = \prod_{j=1}^{N+2} \frac{(z - z_j)}{(z_i - z_j)} = \frac{p_{N+2}(z)}{(z - z_i)p'_{N+2}(z)}, \quad i \neq j, \quad (\text{A14})$$

$$l_i(r) = \prod_{j=1}^{M+1} \frac{(r - r_j)}{(r_i - r_j)} = \frac{q_{M+1}(r)}{(r - r_i)q'_{M+1}(r)}, \quad i \neq j, \quad (\text{A15})$$

and where  $p(z_i)$  and  $q(r_i)$  are values of the solution at the collocation points. Derivatives of the trial solutions at the collocation points are obtained by differentiating Eqs. (A12) and (A13):

$$\frac{dp_{N+2}(z_j)}{dz} = \sum_{i=1}^{N+2} \left[ \frac{dl_i(z)}{dz} \right]_{z_j} p(z_i), \quad (\text{A16})$$

$$\frac{dq_{M+1}(r_j)}{dr} = \sum_{i=1}^{M+1} \left[ \frac{dl_i(r)}{dr} \right]_{r_j} q(r_i). \quad (\text{A17})$$

Michelsen and Villadsen give the following general formulas for the computation of the first derivative of  $l_i(x)$  in terms of derivatives of the node polynomials,

$$l'_i(x_i) = \frac{1}{2} \frac{P''_k(x_i)}{P'(x_i)}, \quad x = x_i, \quad (\text{A18})$$

and

$$l'_i(x_j) = \frac{1}{x_j - x_i} \frac{P'_k(x_j)}{P'_k(x_i)}, \quad x = x_j \neq x_i, \quad (\text{A19})$$

where  $k$  is  $(N+2)$  for the fluid phase with two boundary conditions and  $(M+1)$  for the solid phase with one boundary condition.  $P'_k(x_i)$  and  $P''_k(x_i)$  can be obtained via recursion using

$$P_j(x_i) = (x_i - x_j)P_{j-1}(x_i), \quad (\text{A20})$$

$$P'_j(x_i) = (x_i - x_j)P'_{j-1}(x_i), \quad (\text{A21})$$

$$P''_j(x_i) = (x_i - x_j)P''_{j-1}(x_i) + 2P'_{j-1}(x_i), \quad (\text{A22})$$

where  $j = 1, 2, \dots, k$ ;  $P_0(x_i) = 1$ ; and  $P_1(x_i) = 0$ .

Equations (A18) and (A19) yield vectors of differential operators that act on the values of the solution at the collocation points. The vectors can be expressed as summations that correspond to individual collocation points,  $z_i$  and  $r_i$ . For the fluid phase:

$$p'_{N+2}(z_i) = \sum_{j=1}^{N+2} l'_j(z_i) \cdot p(z_j) = \sum_{j=1}^{N+2} AG_{i,j} \cdot p_j, \quad (AG : \text{fluid phase}) \quad (\text{A23})$$

and for the solid phase,

$$q'_{M+1}(r_i) = \sum_{j=1}^{M+1} l'_j(r_i) \cdot q(r_j) = \sum_{j=1}^{M+1} AS_{i,j} \cdot q_j, \quad (AS : \text{solid phase}) \quad (\text{A24})$$

$\overline{AG}$  and  $\overline{AS}$  are  $(N+2) * (N+2)$  and  $(M+1) * (M+1)$  discretization matrices, which are used to represent  $\partial p / \partial z$  in terms of  $p$  and  $\partial q / \partial r$  in terms of  $q$ . Each

row contains differential operators for one collocation point. Second derivatives may be computed by taking derivatives of Eqs. (A23) and (A24),

$$p''_{N+2}(z_i) = \left. \frac{\partial^2 p}{\partial z^2} \right|_{z=z_i} = \sum_{j=1}^{N+2} AG_{ij} \left[ \sum_{k=1}^{N+2} AG_{jk} \cdot p_k \right], \quad (\text{A25})$$

$$q''_{M+1}(r_i) = \left. \frac{\partial^2 q}{\partial r^2} \right|_{r=r_i} = \sum_{j=1}^{M+1} AS_{ij} \left[ \sum_{k=1}^{M+1} AS_{jk} \cdot q_k \right]. \quad (\text{A26})$$

Note that the derivatives represented by Eqs. (A23) and (A24) are dependent on every collocation point; the second derivatives are dependent on the first derivative at every collocation point.

Equations (A23) through (A26) are equivalent to Eqs. (35) through (38) in the text, and they are in a form that can be substituted into the model equations. A final development of the model equations is given in Sect. 3.3.

## APPENDIX B: FORTRAN COMPUTER CODE

The FORTRAN source listing that begins on the following page was originally written to run on an LMC MegaMicro computer. It was later transported for use on a Digital VAX 11/785 computer, and a Digital PDP-10 computer. With the possible exception of some input/output statements, it conforms to FORTRAN 77 conventions and seems to be transportable.

The subroutines necessary to run the code are included in the listing, except for LSODE and the routines that support it. With twenty-four ODE's to solve, CPU times of about two minutes were typical for N<sub>2</sub> runs on the PDP-10; CO<sub>2</sub> runs required approximately one minute. Of course, solution time depends on the number of equations and the computational difficulty imposed by the problem parameters.

```
C
C
C PROGRAM: SORBQ
C LANG : FORTRAN 77
C BY : JK PRAZNAK
C UPDATED: 10/25/86
C
C USE : SORBQ COMPUTES THE UNSTEADY-STATE PRESSURE PROFILE IN A
C       FIXED BED OF ZEOLITE MOLECULAR SIEVES. THE BED ACTS AS A
C       CRYOSORPTION PUMP. ORTHOGONAL COLLOCATION IS USED TO
C       REDUCE THE SIMULTANEOUS PARABOLIC PDE'S THAT DESCRIBE GAS
C       FLOW AND ADSORPTION TO A SET OF ODE'S. LSODE IS USED TO
C       INTEGRATE THE ODE'S.
C
C       SORBQ SOLVES NTG*NTS SIMULTANEOUS ODE'S, WHERE NTG IS THE
C       NUMBER OF COLLOCATION POINTS FOR THE GAS PHASE AND NTS IS
C       THE NUMBER FOR THE SOLID PHASE.
C
C       CALCULATIONS ARE PERFORMED IN DOUBLE PRECICSION.
C
C VARIABLES:
C   AG = NTG X NTG DISCRETIZATION MATRIX FOR DP/DZ (GAS)
C   ALP = EXPONENT IN JACOBI ORTHOGONALITY RELATIONSHIP
C   AREA = CROSS SECTIONAL AREA OF BED (CM**2)
C   AS = NTS X NTS DISCRETIZATION MATRIX FOR DQ/DR (SOLID)
C   ATOL = 1-VECTOR ABSOLUTE TOLERANCE FOR LSODE
C   AVESPH = AVERAGE SOLID LOADING IN SORBENT PARTICLE (S.P.)
C           (MOL SORBATE/CM**3 S.P.)
C   BET = EXPONENT IN JACOBI ORTHOGONALITY RELATIONSHIP
C   DCOM = NEQ-VECTOR EQUAL TO D IN BED, IN COMMON FOR INFO
C   DELP = COLUMN PRESSURE DROP (TORR)
C   DENB = BULK DENSITY OF MOLECULAR SIEVE (GM MOL SV/CM**3
C         BED)
C   DENSP = DENSITY OF SORBENT PARTICLE (GM S.P./CM**3 S.P.)
C   DIF1,DIF2,DIF3 = NG-VECTOR FIRST, SECOND, THIRD DERIVATIVES
C                   OF JACOBI POLYNOMIAL AT COLLOCATION POINTS
C   DK = KNUDSEN DIFFUSIVITY (CM**2/S)
C   DM = NTG-VECTOR MOLECULAR DIFFUSIVITY (CM**2/S)
C   DP = NTG-VECTOR PORE DIFFUSIVITY (CM**2/S)
C   DPDT = NTG-VECTOR OF TIME DEP. BED PRESSURE DERIVATIVES
C   DQATR = NTG-VECTOR DQ/DR AT SOLID SURFACE
C           ((MOL SRBATE/GM MOL SV)/CM)
C   DQDR = NTS-VECTOR DQ/DR
C   DZ = DIFFUSIVITY IN SOLID (CM**2/S)
C   D0 = LIMITING DIFFUSIVITY IN SOLID (FROM DARKEN EQN.)
C   D2QDR2 = NTS-VECTOR D2Q/DR**2 ((MOL/GM S.P.)/S)
C   D2YDZ2 = NTG-VECTOR D2Y/DZ**2 (DIMENSIONLESS)
C   FLOWIN = MOLES OF SORBATE IN THE BED (FLUX*TIME)
C   GASFRC = FRACTION OF BED AVAILABLE TO GAS
```

C (CM\*\*3 VOID/CM\*\*3 BED)  
 C GASINT = SUM OF GAS IN THE BED (MOLES)  
 C INFLUX = FLUX OF GAS INTO SYSTEM (TORR-L/S)  
 C IPRT = PRINT OUTPUT INDICATOR: 0-MINIMUM OUPPUT,  
 C 1-OUTPUT AT EACH INTEGRATOR TIME STEP,  
 C 2 AND 3-OUTPUT AT EACH CALL TO BED  
 C ISTATE = LSODE SUCCESS INDICATOR  
 C ITASK = LSODE PARAMETER  
 C IWORK = LSODE INTEGER WORK ARRAY  
 C KLANG = EMPIRICAL LANGMUIR CONSTANT (1/TORR)  
 C LENGTH = BED LENGTH (CM)  
 C LIW = LENGTH OF IWORK  
 C LRW = LENGTH OF RWORK  
 C NDIM = ROW DIMENSION OF AS, AG  
 C NEQ = NUMBER ODE'S TO BE SOLVED BY LSODE  
 C NG = NUMBER INTERIOR BED COLLOCATION POINTS  
 C NS = NUMBER INTERIOR SOLID COLLOCATION POINTS  
 C NTG = TOTAL NUMBER BED COLLOCATION POINTS  
 C NTS = TOTAL NUMBER SOLID COLLOCATION POINTS  
 C N0G = INDICATES PRESENCE (1) OR ABSENCE (0) OF  
 C COLLOCATION POINT AT TOP OF BED  
 C N0S = PRESENCE/ABSENCE OF COLL POINT AT SOLID RADIUS = 0  
 C N1G = PRESENCE/ABSENCE OF COLL POINT AT Z = 1  
 C N1S = PRESENCE/ABSENCE OD COLL POINT AT SOLID RADIUS = 1  
 C OMEGA = LENNARD JONES CONSTANT  
 C PERDIF = PERCENT DIFFERENCE BETWEEN FLOWIN AND INTEGRATED  
 C TOTAL SORBATE CALCULATIONS  
 C PIC = INITIAL CONDITIONS  
 C PREF = REFERENCE PRESSURE (TORR)  
 C PRSTEP = INCREMENTAL PRINT TIME (HOURS)  
 C QM = LANGMUIR CONSTANT (MOL SORBATE/GM MOL SV)  
 C RADIUS = SORBENT PARTICLE RADIUS (CM)  
 C RGAS = IDEAL GAS CONSTANT (TORR-CM\*\*3/MOL-K)  
 C RESID = ABSOLUTE DIFFERENCE BETWEEN FLOWIN AND INTEGRATED  
 C TOTAL SORBATE CALCULATIONS  
 C RMW = MOLECULAR WEIGHT OF SORBATE (GM/MOL)  
 C RP = MEAN PORE RADIUS IN BED (CM)  
 C RWORK = REAL WORK VECTOR FOR LSODE  
 C SIGMA = LENNARD JONES COLLISION DIAMETER (ANGSTROMS)  
 C SOLINT = NUMBER MOLES OF ADSORBED SOLID IN BED (MOLES)  
 C SPFRAC = FRACTION OF BED VOLUME OCCUPIED BY SORBENT  
 C PARTICLES (CM\*\*3 S.P./CM\*\*3 BED)  
 C SUMCOL = SUM OF ADSORBED SOLID IN BED (MOLES)  
 C SUMG = SUM OF GAS IN BED (MOLES)  
 C SUMTOT = SUM OF TOTAL SORBATE (GAS AND SOLID) IN BED  
 C (MOLES)  
 C TAMB = AMBIENT TEMPERATURE (K)  
 C TBED = TEMPERATURE IN BED (K)  
 C TCRIT = OVERSHOOT TOLERANCE ON TOUT FOR LSODE (S)

C TFINAL = ENDING TIME (S)  
C THRESH = INITIAL PRINT TIME, INCREMENTED BY PRSTEP (HRS)  
C THRS = TIME (HRS)  
C TOUT = INTEGRATOR TIME (S)  
C VA = VECTOR RETURNED FROM DFOPR CONTAINING ROWS OF  
C DISCRETIZATION MATRIX  
C VOL = VOLUME OF HEADSPACE ABOVE BED (CM\*\*3)  
C WG = NTG-VECTOR OF GAUSSIAN WEIGHTS FOR BED COLL.  
C POINTS  
C WS = NTS-VECTOR OF GAUSSIAN WEIGHTS FOR SOL COLL.  
C POINTS  
C WSSUM = SUM OF WS  
C WGSUM = SUM OF WG  
C XG = NTG-VECTOR OF BED COLLOCATION POINTS  
C XS = NTS-VECTOR OF SOLID COLLOCATION POINTS  
C Y = NEQ-VECTOR OF DEPENDENT VARIABLES  
C YG = NTG-VECTOR OF DIMENSIONLESS GAS PRESSURES  
C YS = NTS X NTS MATRIX OF DIMENSIONLESS SOLID LOADINGS

C SUBROUTINE CALLS:

C  
C BED COMPUTES THE FIRST DERIVATIVES OF THE DEPENDENT  
C VARIABLE REQUIRED BY LSODE. JAC WOULD COMPUTE THE JACOBIAN  
C MATRIX, HOWEVER, THE JACOBIAN IS COMPUTED NUMERICALLY BY  
C LSODE IN THIS CODE. JCOBI COMPUTES COLLOCATION POINTS.  
C DFOPR COMPUTES THE DIFFERENTIAL OPERATORS, OR  
C DISCRETIZATION MATRICES, AND GAUSSIAN WEIGHTS. LSODE  
C INTEGRATES THE SYSTEM OF ODE'S FORMED BY BED.

C DIMENSIONING INFORMATION:

C  
C Y MUST BE DIMENSIONED TO AT LEAST NEQ. DIF1, DIF2, DIF3,  
C AND VA MUST BE DIMENSIONED AT LEAST TO THE LARGER OF NTG  
C OR NTS. AG, XG, WG, YG, DPDT, D2YD2Z, DQATR, DQDR, DM, DP  
C AND THE FIRST DIMENSION OF YS MUST BE AT LEAST NTG.  
C AS, XS, WS AND THE SECOND DIMENSION OF YS MUST BE AT  
C LEAST NTS.

C  
C RWORK MUST BE DIMENSIONED TO AT LEAST (22 + 9\*NEQ +  
C NEQ\*\*2).

C IWORK MUST BE AT LEAST (NEQ+20).

C REFERENCES:

C  
C LSODE - LIVERMORE SOLVER FOR ORDINARY DIFFERENTIAL  
C EQUATIONS. DOCUMENTATION INCLUDED WITH CODE. CODE  
C OBTAINED FROM MARTIN MARIETTA ENERGY SYSTEMS,  
C COMPUTING AND TELECOMMUNICATIONS DIVISION CORE LIBRARY.

C

C MICHELSEN AND VILLADSEN, SOLUTION OF DIFFERENTIAL EQUATION  
 C MODELS BY POLYNOMIAL APPROXIMATION, 1982.

C  
 IMPLICIT REAL\*8 (A-H,O-Z)  
 REAL\*8 LENGTH, INFLUX, KLANG  
 CHARACTER FNAME\*10  
 DIMENSION Y(40), RWORK(2000), IWORK(60), ATOL(1)  
 DIMENSION DIF1(15), DIF2(15), DIF3(15), VA(15)  
 COMMON/COLLG/ AG(15,15), XG(15), WG(15)  
 COMMON/COLLS/ AS(15,15), XS(15), WS(15)  
 COMMON/BEDCON/LENGTH, DENB, DENSP, TAMB, GASFRAC, VOL, RADIUS,  
 1 QM, SPFRAC, RGAS, TBED, PREF, AREA, D0, KLANG, INFLUX  
 COMMON/ICONST/NTG, NTS, NDIM, ITERM, IOUT, IPRT  
 COMMON/DERVS/ DCOM(40), D2YDZ2(15), D2QDR2(15,15), DQATR(15),  
 1 DQDR(15)  
 COMMON/PARMS/YG(10), YS(10,10), DPDT(10)  
 COMMON/PARMS2/DZ, RMW, RP, SIGMA, OMEGA, DK, DM(10), DP(10)  
 EXTERNAL BED,JAC

C  
 C OPEN DATA FILE AND READ CONSTANTS

C  
 OPEN (21, FILE='SORBQ.DAT', STATUS='OLD')  
 OPEN (22, FILE='SORBQ.PLO', STATUS='OLD')  
 READ(21,905) NG,NS  
 NOG = 1  
 N1G = 1  
 NOS = 0  
 N1S = 1  
 NTG = NG + NOG + N1G  
 NTS = NS + NOS + N1S  
 NEQ = NTG\*(NTS)  
 READ(21,804) FNAME  
 READ(21,906) TOUT,TFINAL  
 OPEN(24, FILE=FNAME, STATUS='OLD')

C  
 READ(21,800) ITOL, ITASK, ISTATE, IOPT, LRW, LIW, MF  
 READ(21,801) T, RTOL, ATOL(1), TCRT  
 READ(21,801) LENGTH, DENB, DENSP, TAMB, VOL, RADIUS, QM  
 READ(21,801) RGAS, TBED, PREF, AREA, KLANG, INFLUX  
 READ(21,802) D0, RMW, RP, SIGMA, OMEGA  
 READ(21,801) GASFRAC, SPFRAC  
 READ(21,800) NDIM, ITERM, IOUT, IPRT  
 READ(21,801) THRESH, PRSTEP  
 READ(21,801) PIC

C  
 C ECHO DATA TO TERMINAL OR OUTPUT FILE

C  
 WRITE(22,799)  
 799 FORMAT('05DUMY\$')

```

WRITE(IOUT,921)
WRITE(IOUT,922) LENGTH, AREA, TBED
WRITE(IOUT,923) VOL, INFLUX, TAMB
WRITE(IOUT,924)
WRITE(IOUT,925) RADIUS, D0, RP, SIGMA, OMEGA
WRITE(IOUT,926) QM, KLANG
WRITE(IOUT,927) DENB, DENSP, RGAS
WRITE(IOUT,928) GASFRAC, SPFRAC
WRITE(IOUT,929)
WRITE(IOUT,930) NDM, ITERM, IOUT, IPRT
WRITE(IOUT,931) PRSTEP, THRESH
WRITE(IOUT,932) ITOL, ITASK, ISTATE, IOPT
WRITE(IOUT,933) LRW, LIW, MF, RTOL, ATOL(1)
WRITE(IOUT,934) PIC
C
C COMPUTE COLLOCATION POINTS, DISCRETIZATION MATRICES, AND
C WEIGHTS FOR GAS (BED) AND SOLID (ZEOLITE)
C
C GAS - PLANAR GEOMETRY, BOTH ENDPOINTS REQUIRED (N0G=N1G=1)
C
  ALP = 0.D0
  BET = 0.D0
  CALL JCOBI(NDIM,NG,N0G,N1G,ALP,BET,DIF1,DIF2,DIF3,XG)
  DO 5 I = 1,NTG
    CALL DFOPR(NDIM,NG,N0G,N1G,I,1,DIF1,DIF2,DIF3,XG,VA)
    DO 4 J = 1,NTG
      4 AG(I,J) = VA(J)
    5 CONTINUE
    CALL DFOPR(NDIM,NG,N0G,N1G,I,3,DIF1,DIF2,DIF3,XG,WG)
C
C SOLID - ONE ENDPOINT INCLUDED, COLLOCATION POINTS COMPUTED
C USING PLANAR GEOMETRY
C
  ALP = 0.D0
  BET = 0.D0
  CALL JCOBI(NDIM,NS,N0S,N1S,ALP,BET,DIF1,DIF2,DIF3,XS)
  DO 7 I = 1,NTS
    CALL DFOPR(NDIM,NS,N0S,N1S,I,1,DIF1,DIF2,DIF3,XS,VA)
    DO 6 J = 1,NTS
      6 AS(I,J) = VA(J)
    7 CONTINUE
    CALL DFOPR(NDIM,NS,N0S,N1S,I,3,DIF1,DIF2,DIF3,XS,WS)
C
C PRINT POINTS AND WEIGHTS TO DATA FILE
C
  WRITE(IOUT,905) NG,NS
  WRITE(IOUT,906) (XG(I),I=1,NTG)
  WRITE(IOUT,906) (WG(I),I=1,NTG)
  WRITE(IOUT,906) (XS(I),I=1,NTS)

```

```

      WRITE(IOUT,906) (WS(I),I=1,NTS)
C
C SET INITIAL CONDITIONS
C
      DO 30 I = 1,NTG
        II = (I-1)*NTS + 1
        Y(II) = PIC
        DO 20 J = 1,NTS-1
          JJ = II + J
        20 Y(JJ) = PIC
      30 CONTINUE
C
C RWORK(1) IS THE TIME BEYOND WHICH LSODE WILL NOT INTEGRATE IN THE
C CURRENT STEP. IT APPLIES ONLY IF ITASK = 4 OR 5.
C
      RWORK(1) = TOUT + TCRIT
C
C CALL INTEGRATOR AND WRITE RESULTS
C
      40 CALL LSODE(BED, NEQ, Y, T, TOUT, ITOL, RTOL, ATOL, ITASK,
        1 ISTATE, IOPT, RWORK, LRW, IWORK, LIW, JAC, MF)
C
C OUTPUT FOR DEBUGGING: IPRT = 0; NO PRINTED OUTPUT
C      IPRT = 1; OUTPUT EACH CALL TO LSODE
C      IPRT > 1; OUTPUT EACH CALL TO BED
C
      IF(IPRT .GE. 1) THEN
        WRITE(ITERM,907) RWORK(13)
        WRITE(ITERM,908) RWORK(11), RWORK(12), IWORK(14), IWORK(15)
        WRITE(ITERM,909) IWORK(11), IWORK(12), IWORK(13)
      C
      C Y,Q,DYDT,DQDT AT TOP OF BED
        WRITE(ITERM,910) Y(1), Y(2), Y(NTS), D(1), D(2), D(NTS)
      C
      C Y,Q,DYDT,DQDT AT BOTTOM OF BED
        NLAST = (NTG-1)*NTS
        WRITE(ITERM,911) Y(NLAST+1),Y(NLAST+2),Y(NLAST+NTS),
          D(NLAST+1),D(NLAST+2),D(NLAST+NTS)
        ENDIF
      C
      C COMPUTE AMOUNT OF SORBATE IN BED BY INTEGRATING GAS AND SOLID
      C LOADING USING GAUSSIAN QUADRATURE
      C
        SUMG = 0.D0
        SUMCOL = 0.D0
        WGSUM = 0.D0
        DO 50 I = 1,NTG
          AVESPH = 0.D0
          WSSUM = 0.D0

```

```

DO 45 J = 1,NTS
AVESPH = AVESPH + WS(J)*YS(I,J)*XS(J)*XS(J)
WSSUM = WSSUM + WS(J)
45 CONTINUE
AVESPH = (3.D0*QM*DENB/SPFRAC*AVESPH) /WSSUM
SUMCOL = SUMCOL + WG(I)*AVESPH*SPFRAC*AREA*LENGTH
WGSUM = WGSUM + WG(I)
SUMG = SUMG + PREF*AREA/(RGAS*TBED) * WG(I)*YG(I)
50 CONTINUE
SUMCOL = SUMCOL/WGSUM
SUMG = SUMG/WGSUM
SUMTOT = SUMG + SUMCOL
C
C SUMMARIZE INTEGRALS OF GAS AND SOLID PROFILES; COMPUTE DIFFERENCE
C BETWEEN TOTAL FED AND COMPUTED ACCUMULATION
C
FLOWIN = INFLUX*1000.D0/RGAS/TAMB * T
GASINT = SUMG
SOLINT = SUMCOL
RESID = SUMTOT - FLOWIN
IF(INFLUX .NE. 0.D0) PERDIF = RESID*100.D0/FLOWIN
C
C CHECK RESULT
C
IF(ISTATE .LT. 0) THEN
WRITE(ITERM,914) ISTATE,T,IWORK(11),IWORK(12),IWORK(13)
STOP
ELSEIF(TOUT .GE. TFINAL) THEN
WRITE(ITERM,915) IWORK(11), IWORK(12), IWORK(13)
STOP
ELSE
TOUT = TOUT + RWORK(12)
RWORK(1) = TOUT + TCRIT
C
C WRITE TO DATA FILE
C
THRS = TOUT/3600.D0
IF(THRS .GE. THRESH) THEN
THRESH = THRESH + PRSTEP
DELP = YG(1) - YG(NTG)
WRITE(22,918) THRS, YG(1), DELP
WRITE(IOUT,916) THRS, YG(1), DELP, FLOWIN, RESID, PERDIF
C # WRITE(IOUT,917) (YG(I), I=1,NTG)
WRITE(IOUT,919) DZ, (DP(I),I=1,NTG)
DO 60 I = 1,NTG
60 WRITE(IOUT,917) (YS(I,J), J = 1,NTS)
ENDIF
C
GO TO 40

```

```

      ENDIF
C
      STOP
800 FORMAT((15X,I5))
801 FORMAT((10X,F10.0))
802 FORMAT(10X,D10.2)
803 FORMAT(I2)
804 FORMAT(A10)
805 FORMAT((F10.0))
901 FORMAT(1H , 'ENTER THE NUMBER OF INTERIOR COLLOCATION POINTS'/
      1 1H , 'FOR THE BED (NG) AND THE SOLID (NS):')
902 FORMAT(1H , 'ENTER NAME OF OUTPUT FILE (MAX 10 CHARACTERS):')
903 FORMAT(1H , 'ENTER INITIAL OUTPUT POINT, AND TFINAL (SECS):')
905 FORMAT(16I5)
906 FORMAT(8(F10.8))
907 FORMAT(/1H , 'AT INT TIME = ',F12.3, ' SECS:')
908 FORMAT(1H , ' LAST T-STEP = ',F10.4, ' NEXT T-STEP = ',F10.4,/
      1 1H , ' LAST ORDER = ',I2,8X, ' NEXT ORDER = ',I2)
909 FORMAT(1H , ' NO. STEPS = ',I4, ' NFE = ',I4, ' NJE = ',I4)
910 FORMAT(1H , 'AT Z=0, P:',F10.5, ' Q(1): ',F10.8, ' Q(NS):',
      1 F10.8/
      2 1H , ' DP:',G10.4, ' DQ(1): ',G10.4, ' DQ(NS):',
      3 G10.4)
911 FORMAT(1H , 'AT Z=L, P:',F10.5, ' Q(1): ',F10.8, ' Q(NS):',
      1 F10.8/
      2 1H , ' DP:',G10.4, ' DQ(1): ',G10.4, ' DQ(NS):',
      3 G10.4)
914 FORMAT(1H , 'ERROR TERMINATION: ISTATE = ',I3, ' T = ',F15.5,/,
      1 1H , ' NO. STEPS = ',I4, ' NO. FE = ',I4, ' NO. JE=',
      2 I4)
915 FORMAT(1H , 'END OF RUN SUMMARY:',/,
      1 1H , ' NO. STEPS = ',I4, ' NO. FE = ',I4, ' NO. JE =',
      2 I4)
916 FORMAT(F10.6,2(F10.5),F10.6,F10.6,F10.4)
917 FORMAT(8(F10.8))
918 FORMAT(F10.5,2F10.6,2F10.8)
919 FORMAT(8(F10.5))
920 FORMAT(1H ,5(F11.7,1X))
921 FORMAT(///1H , 'BED PARAMETERS:')
922 FORMAT(1H , 'LENGTH = ',F7.3, ' CM',T30, 'CS AREA = ',F7.4,
      1 ' CM**2',T60, 'BED TEMP = ',F6.2, ' K')
923 FORMAT(1H , 'HEADSPACE = ',F8.2, ' CM**3',T30, 'INFLUX = ',E11.5,
      1 ' TR-L/S',T60, 'AMB TEMP = ',F6.2, ' K')
924 FORMAT(/1H , 'SORBENT PARAMETERS:')
925 FORMAT(1H , 'EFFECTIVE CRYSTAL RADIUS = ',E11.5, ' CM',/,
      1 1H , 'LIMITING ZEOLITE DIFFUSIVITY = ',E11.3, ' CM**2/S',/,
      2 1H , 'BED DIFFUSIVITY CONSTANTS:',/,
      3 1H , ' EFFECTIVE PORE RADIUS (RP) = ',F8.6, ' CM',/,
      4 1H , ' LENNARD-JONES SIGMA = ',F8.6, ' A',/,

```

```

5 1H , 'LENNARD-JONES OMEGA = ',F8.6,/)
926 FORMAT(1H , 'ISOTHERM CONSTANTS: QM = ',F9.5, 'MOL/GM',5X,
1 'K = ',F8.5, '1/TORR')
927 FORMAT(1H , 'BULK DENSITY = ',F7.3, 'GM MOL SV/CM**3 BED'/
1 1H , 'SORBENT PART. DENSITY = ',F7.3, 'GM S.P./CM**3 S.P.:/
2 1H , 'GAS CONSTANT = ',F9.2, 'TORR-CM**3/MOLE-K')
928 FORMAT(/1H , 'FRACTION OF COLUMN AVAILABLE FOR GAS = ',F5.3,
1 ' CM**3 GAS/CM**3 BED',/,
2 1H , 'FRACTION OF COLUMN OCCUPIED BY CRYSTALS = ',F5.3,
3 ' CM**3 CRYSTALS/CM**3 BED')
929 FORMAT(/1H , 'PROBLEM PARAMETERS:')
930 FORMAT(1H , 'NDIM = ',I2,T20, 'ITERM = ',I2,T40, 'IOUT = ',I2,T60,
1 'IPRT = ',I1)
931 FORMAT(1H , 'PRINT STEP = ',F5.2, 'HRS',T40, 'INITIAL PRT TIME = '
1 ,F7.2, 'HRS')
932 FORMAT(/1H , 'ITOL = ',I1,T20, 'ITASK = ',I1,T40, 'ISTATE = ',I1,
1 T60, 'IOPT = ',I1)
933 FORMAT(1H , 'LRW = ',I4,T20, 'LIW = ',I4,T40, 'MF = ',I2,T60,
1 'RTOL = ',E8.2,/,1H , 'ATOL = ',E8.2)
934 FORMAT(/1H , 'INITIAL CONDITION ON BED: ',/
1 ' PRESSURE = ',F7.5, 'TORR'/)
END

```

C

C

SUBROUTINE BED(NEQ, T, Y, D)

C

C

C NAME: BED

C

C USE : BED COMPUTES NEQN FIRST-ORDER ODE'S THAT DESCRIBE THE TRANS-  
C IENT GAS PRESSURE AND SOLID LOADING PROFILES THROUGH A FIXED BED  
C OF MOLECULAR SIEVES THAT ACT AS A CRYOSORPTION PUMP. THE  
C DERIVATIVES WITH RESPECT TO AXIAL BED POSITION ARE ESTIMATED  
C USING ORTHOGONAL COLLOCATION.

C

C VARIABLES (SEE ALSO LIST IN MAIN PROGRAM):

C

C D = NEQ-VECTOR OF TIME-DEPENDENT DERIVATIVES  
C (COMPUTED BY BED AND PASSED TO LSODE)  
C DCOM = EQUIVALENT OF D, PASSED TO MAIN ROUTINE FOR INFO  
C DK = KNUDSEN DIFFUSIVITY (CM\*\*2/S)  
C DM = NTG-VECTOR OF MOLECULAR DIFFUSIVITY (CM\*\*2/S)  
C DP = OVERALL PORE DIFFUSIVITY (CM\*\*2/S)  
C DPOIS = POISEUILLE FLOW CONTRIBUTION TO DIFFUSIVITY  
C (CM\*\*2/S)  
C DY1DT = SEPARATELY COMPUTED VALUE OF DY(1)/DT  
C DY1FAC = CONSTANT FACTOR IN COMPUTATION OF DY(1)/DT  
C DY1DZ = SEPARATELY COMPUTED VALUE OF DY/DZ AT Z=0  
C EPRTL2 = CONSTANT COEFFICIENT OF D2Y/DZ\*\*2

```

C   EAPRTL = CONSTANT COEFFICIENT OF DY/DZ AT Z=0
C   NEQ = NUMBER OF ODE'S
C   RTEP = INVERTED CONSTANT COEFFICIENT OF DY/DT
C   SPCON = SORBENT PARTICLE CONSTANT (GM S.P./CM**3 BED)
C   T = TIME PASSED BY LSODE (S)
C   VPRT = CONSTANT COEFFICIENT OF DY/DT (HEADSPACE)
C   Y = NEQ-VECTOR OF DEPENDENT VARS PASSED TO BED
C   YG = NTG-VECTOR OF DIMENSIONLESS GAS PRESSURES
C   YS = NTG X NTS MATRIX OF DIMENSIONLESS SOLID LOADINGS
C   (YG AND YS DEFINED FROM Y FOR CONVENIENCE)
C
C
C   _____
C   IMPLICIT REAL*8 (A-H,O-Z)
C   REAL*8 LENGTH, INFLUX, KLANG
C   DIMENSION Y(NEQ), D(NEQ)
C   COMMON/COLLG/ AG(15,15), XG(15), WG(15)
C   COMMON/COLLS/ AS(15,15), XS(15), WS(15)
C   COMMON/BEDCON/LENGTH, DENB, DENSP, TAMB, GASFRC, VOL,RADIUS,QM,
C   1 SPFRAC, RGAS, TBED, PREF, AREA, DO, KLANG, INFLUX
C   COMMON/ICONST/NTG, NTS, NDIM, ITERM, IOUT, IPRT
C   COMMON/DERVS/ DCOM(40), D2YDZ2(15), D2QDR2(15,15), DQATR(15),
C   1 DQDR(15)
C   COMMON/PARMS/YG(10), YS(10,10)
C   COMMON/PARMS2/DZ, RMW, RP, SIGMA, OMEGA, DK, DM(10), DP(10)
C
C
C   COMPUTE CONSTANTS FOR USE IN EQUATIONS
C
C   RTEP = RGAS*TBED/GASFRC/PREF
C   VPRT = VOL*PREF/RGAS/TAMB
C   EPRTL2 = GASFRC*PREF/RGAS/TBED/LENGTH**2
C   EAPRTL = EPRTL2*AREA*LENGTH
C   SPCON = DENB
C
C
C   LOAD Y INTO SEPARATE ARRAYS, ONE FOR GAS AND ONE FOR SOLIDS AT EACH
C   GAS POINT. ALSO COMPUTE AND INCLUDE CONCENTRATION OF SOLID AT THE
C   SURFACE OF THE SPHERES AT EACH GAS POINT - A BOUNDARY CONDITION.
C
C   DO 20 I = 1,NTG
C     LOC = (I-1)*NTS + 1
C     YSNTS = KLANG*PREF*Y(LOC)/(1.DO+KLANG*PREF*Y(LOC))
C     YG(I) = Y(LOC)
C     DO 10 J = 1,NTS-1
C       10 YS(I,J) = Y(LOC+J)
C     YS(I,NTS) = YSNTS
C   20 CONTINUE
C
C
C   COMPUTE EFFECTIVE PORE DIFFUSIVITY (DP) BASED ON CONTRIBUTIONS
C   FROM KNUDSEN DIFFUSIVITY (DK), MOLECULAR DIFFUSIVITY (DM), AND
C   POISEUILLE FLOW (DPOIS). DM, DP, AND DPOIS ARE FUNCTIONS OF

```

## C GAS PRESSURE

C

```

DK = 9700.D0*RP*SQRT(TBED/RMW)
DMP = 0.00158D0*760.D0*SQRT(TBED**3 * 2.D0/RMW)
DMP = DMP/SIGMA/SIGMA/OMEGA
VIS = 2.6693D-5*DSQRT(RMW*TBED)/SIGMA/SIGMA/OMEGA
DO 30 I = 1,NTG
IF(YG(I) .NE. 0.D0) THEN
DM(I) = DMP/YG(I)/PREF
DPOIS = 1333.2D0*RP*RP/(8.D0*VIS) * YG(I)*PREF
DP(I) = 1.D0/(1.D0/DK + 1.D0/DM(I)) + DPOIS
ELSE
DP(I) = DK
ENDIF
30 CONTINUE

```

C

C COMPUTE FIRST AND SECOND DERIVATIVES OF SOLID CONCENTRATION

C FOR EACH POINT IN THE COLUMN

C

```

DO 70 I = 1,NTG
DQATR(I) = 0.D0
DO 60 J = 1,NTS
DZ = D0/(1.D0 - YS(I,NTS))
DQATR(I) = DQATR(I) + (QM/RADIUS)*(3.D0*DZ/RADIUS)
1 *AS(NTS,J)*YS(I,J)
DENOM = RADIUS*RADIUS*XS(J)*XS(J)
D2QDR2(I,J) = 0.D0
DO 50 K = 1,NTS
DQDR(K) = 0.D0
DO 40 L = 1,NTS
40 DQDR(K) = DQDR(K) + AS(K,L)*YS(I,L)
DZ = D0/(1.D0 - YS(I,K))
50 D2QDR2(I,J) = D2QDR2(I,J) + DZ*XS(K)**2*AS(J,K)*DQDR(K)
1 /DENOM
60 CONTINUE
70 CONTINUE

```

C

C COMPUTE DERIVATIVES OF PRESSURE AND AND ODE'S

C

C COMPUTE FLUID-PHASE BALANCE AT Z=0, INCLUDING BOUNDARY CONDITION

C WITH ASSUMPTION THAT  $DY_1/DT = DY(\text{HEAD SPACE})/DT$ 

C

```

DY1FAC = 1.D0/(1.D0 - RTEP*EPRTL2/EAPRTL*VPRT*AG(1,1))
D2YDZ2(1) = 0.D0
DO 90 I = 2,NTG-1
DYDZ = 0.D0
DO 80 J = 1,NTG
80 DYDZ = DYDZ + AG(I,J)*YG(J)
90 D2YDZ2(1) = D2YDZ2(1) + AG(1,1)*DYDZ

```

```

D2YDZ2(1) = D2YDZ2(1) - AG(1,1)*INFLUX*1000.D0/RGAS/TAMB
1 /EAPRTL/DP(1)
DY1DT = DY1FAC*(RTEP*(EPRTL2*DP(1)*D2YDZ2(1) - SPCON*DQATR(1)))
C
C NOW COMPUTE REMAINING PRESSURE DERIVATIVES
C
DY1DZ = (VPRT*DY1DT - INFLUX*1000.D0/RGAS/TAMB)/EAPRTL/DP(1)
DO 120 I = 2,NTG
PARTA = AG(I,1)*DY1DZ
PARTB = 0.D0
DO 110 J = 2,NTG-1
DYDZ = 0.D0
DO 100 K = 1,NTG
100 DYDZ = DYDZ + AG(J,K)*YG(K)
110 PARTB = PARTB + AG(I,J)*DYDZ
120 D2YDZ2(I) = PARTA + PARTB
C
C COMPUTE ODE'S
C I => EQN. NO. ; J => BED COLL. POINT ; K => SOLID COLL. POINT
C
DO 140 J=1,NTG
I = (J-1)*NTS + 1
IF(I.EQ. 1) THEN
D(1) = DY1DT
DCOM(1) = D(1)
ELSE
D(I) = RTEP*(EPRTL2*DP(J)*D2YDZ2(J) - SPCON*DQATR(J))
DCOM(I) = D(I)
ENDIF
DO 130 K = 1,NTS-1
I = I + 1
D(I) = D2QDR2(J,K)
130 DCOM(I) = D(I)
140 CONTINUE
C
C OUTPUT FOR DEBUGGING: IPRT = 0; NO OUTPUT
C IPRT = 2; SINGLE LINE OF GAS INFO
C IPRT = 3; TWO LINES, GAS AND SOLID INFO
C
IF(IPRT.EQ.2 .OR. IPRT.EQ.3) THEN
TH = T/3600.D0
JJ = (NTG-1)*(NTS) + 1
DYLDZ = 0.D0
DO 150 I = 1,NTS
150 DYLDZ = DYLDZ + AG(NTG,I)*YG(I)
WRITE(ITERM,951) TH,YG(1),DY1DZ,D(1),YG(NTG),DYLDZ,D(JJ)
IF(IPRT.EQ. 3) THEN
DZ1 = D0/(1.D0-YS(1,NTS))
DZNTG = D0/(1.D0-YS(NTG,NTS))

```



```

DIF2(I) = (AB+AP+Z1)/Z/Z/(Z+1.D0)
GO TO 10
11 Z = Z*Z
Y = Z1*(AB+Z1)
Y = Y*(AP+Y)
DIF2(I) = Y/Z/(Z-1.D0)
10 CONTINUE
C
C ROOT DETERMINATION BY NEWTON'S METHOD WITH SUPPRESSION OF
C PREVIOUSLY DEFINED ROOTS
C
15 X = 0.D0
DO 20 I = 1,N
25 XD = 0.D0
XN = 1.D0
XD1 = 0.D0
XN1 = 0.D0
DO 30 J = 1,N
XP = (DIF1(J)-X)*XN - DIF2(J)*XD
XP1 = (DIF1(J)-X)*XN1 - DIF2(J)*XD1 - XN
XD = XN
XD1 = XN1
XN = XP
30 XN1 = XP1
ZC = 1.D0
Z = XN/XN1
IF (I .EQ. 1) GO TO 21
DO 22 J = 2,I
22 ZC = ZC - Z/(X-ROOT(J-1))
21 Z = Z/ZC
X = X-Z
IF(DABS(Z) .GT. 1.D-9) GO TO 25
ROOT(I) = X
X = X+0.0001D0
20 CONTINUE
C
C ADD EVENTUAL INTERPOLATION POINTS AT X=0 OR X=1
C
NT = N+N0+N1
IF (N0 .EQ. 0) GO TO 35
DO 31 I = 1,N
J = N+1-I
31 ROOT(J+1) = ROOT(J)
ROOT(1) = 0.D0
35 IF (N1 .EQ. 1) ROOT(NT) = 1.D0
C
C NOW EVALUATE DERIVATIVES OF POLYNOMIAL
C
DO 40 I = 1,NT

```

```

X = ROOT(I)
DIF1(I) = 1.D0
DIF2(I) = 0.D0
DIF3(I) = 0.D0
DO 40 J = 1,NT
IF (J .EQ. I) GO TO 40
Y = X - ROOT(J)
DIF3(I) = Y*DIF3(I) + 3.D0*DIF2(I)
DIF2(I) = Y*DIF2(I) + 2.D0*DIF1(I)
DIF1(I) = Y*DIF1(I)
40 CONTINUE
RETURN
END
C
SUBROUTINE DFOPR(ND, N, N0, N1, I, ID, DIF1,DIF2,DIF3, ROOT,
1 VEC)
C
C
C NAME: DFOPR
C BY : VILLADSEN/MICHELSSEN
C
C USE: TO EVALUATE DISCRETIZATION MATRICES OF JACOBI POLYNOMIAL
C DEFINED BY JCOBI. ALSO EVALUATE GAUSSIAN QUADRATURE WEIGHTS.
C
C ID = 1 : DISCRETIZATION MATRIX A
C ID = 2 : DISCRETIZATION MATRIX B
C ID = 3 : GAUSSIAN QUADRATURE WEIGHTS (NORMALIZED TO 1)
C
C
C
C IMPLICIT REAL*8 (A-H,O-Z)
C DIMENSION DIF1(ND), DIF2(ND), DIF3(ND), ROOT(ND), VEC(ND)
C
C NT = N+N0+N1
C IF (ID .EQ. 3) GO TO 10
C DO 20 J = 1,NT
C IF (J .NE. I) GO TO 21
C IF (ID .NE. 1) GO TO 5
C VEC(I) = DIF2(I)/DIF1(I)/2.D0
C GO TO 20
C 5 VEC(I) = DIF3(I)/DIF1(I)/3.D0
C GO TO 20
C 21 Y = ROOT(I) - ROOT(J)
C VEC(J) = DIF1(I)/DIF1(J)/Y
C IF (ID .EQ. 2) VEC(J) = VEC(J)*(DIF2(I)/DIF1(I)-2.D0/Y)
C 20 CONTINUE
C GO TO 50
C
C 10 Y = 0.D0
C DO 25 J = 1,NT

```

```
X = ROOT(J)
AX = X*(1.D0-X)
IF (N0 .EQ. 0) AX = AX/X/X
IF (N1 .EQ. 0) AX = AX/(1.D0-X)/(1.D0-X)
VEC(J) = AX/DIF1(J)**2
25 Y = Y+VEC(J)
DO 60 J = 1,NT
60 VEC(J) = VEC(J)/Y
50 RETURN
END
```



**INTERNAL DISTRIBUTION**

1. L. H. Bell
- 2-6. C. H. Byers
7. J. E. Dunn Jr.
8. P. W. Fisher
9. E. L. Fuller
10. M. R. Gibson
11. M. T. Harris
12. J. R. Hightower
13. E. K. Johnson
14. J. R. Merriman
15. J. J. Perona
- 16-20. J. K. Prazniak
21. C. D. Scott
22. T. C. Scott
23. M. G. Stewart
24. J. S. Watson
25. R. G. Wymer
26. A. D. Zucker
- 27-28. Central Research Library
- 29-30. Laboratory Records
31. Laboratory Records, ORNL R.C.
32. ORNL Patent Section
33. ORNL-Y-12 Technical Library  
Document Reference Section

**EXTERNAL DISTRIBUTION**

34. K. S. Crabb, Rohm and Haas Company, P.O. Box 584,  
Bristol PA 19007
35. H. Cullingford, NASA Johnson Space Center, Crew Systems Division  
EC 231, Houston, TX 77058
36. G. M. Haas, Office of Fusion Energy, DOE Room J-213/GTN,  
Washington, DC 20545
37. R. F. Hirsch, Office of Basic Energy Sciences, DOE, Room G-339/GTN,  
Washington, DC 20545
38. R. S. Marianelli, Office of Basic Energy Sciences, DOE, Room G-338/GTN,  
Washington, DC 20545
39. F. D. Stevenson, Office of Basic Energy Sciences, DOE, Room G-341/GTN,  
Washington, DC 20545
40. Office of Assistant Manager for Energy Research and Development,  
DOE-ORO, P.O. Box E, Oak Ridge, TN 37831
- 41-70. Technical Information Center, Oak Ridge, TN 37831

